JAERI - M
89-192

PROGRESS REPORT ON SAFETY RESEARCH OF HIGH-LEVEL WASTE MANAGEMENT FOR THE PERIOD APRIL 1988 TO MARCH 1989

November 1989

(Eds.) Haruto NAKAMURA and Susumu MURAOKA

日 本 原 子 力 研 究 所
Japan Atomic Energy Research Institute

JAERI-Mレポートは，日本原子力研究所が不定期に公刊している研究報告書です。
入手の問合わせは，日本原子力研究所技術情報部情報資料課（〒319-11茨城県那珂郡東海村）あて，お申しこしください。なお，このほかに財団法人原子力弘済会資料センター（〒319-11 茨城県那珂郡東海村日本原子力研究所内）で複写による実費頒布をおこなっております。

JAERI-M reports are issued irregularly.
Inquiries about availability of the reports should be addressed to Information Division, Department of Technical Information, Japan Atomic Energy Research Institute, Tokai-mura, Naka-gun, Ibaraki-ken 319-11, Japan.

編集兼発行　日本原子力研究所
印　　刷　㈱原子力資料サービス

JAERI-M 89-192

Progress Report on Safety Research of High-Level Waste Management for the Period April 1988 to March 1989

(Eds.) Haruto NAKAMURA and Susumu MURAOKA

Department of Environmental Safety Research
Tokai Research Establishment
Japan Atomic Energy Research Institute
Tokai-mura, Naka-gun, Ibaraki-ken

(Received October 23, 1989)

Researches on high-level waste management at the High Level Waste Management Laboratory and the Waste Safety Testing Facility Operation Division of the Japan Atomic Energy Research Institute in the fiscal year of 1988 are reviewed.

The topics are following studies on the long-term chemical behaviors of long-lived nuclides in geosphere.

1) Mineralogical researches on the alteration layer of glass exposed to water were carried out by laboratory experiments and investigation of natural glass. Leaching experiments of Pu and Np were also conducted.
2) The spectroscopic methods are applied to study the long-term reaction path modeling of radionuclide fixation using natural materials.

Keywords: High-level Radioactive Waste, Glass, Mineralogical Research, Leaching, Plutonium, Neptunium, Spectroscopic Method, Long-term Reaction Path, Fixation

JAERI－M 89－192

高レベル廃棄物処理処分の安全性に関する昭和63年度報告書

日本原子力研究所東海研究所環境安全研究部
（編）中村　治人・村岡　　進

（１９８９年10月23日受理）

日本原子力研究所高レベル廃棄物処理処分研究室及びＷＡＳＴＥＦ管理室で昭和63年度に実施した高レベル廃棄物処理処分に関する研究をまとめたものである。

そのトピックスは地層環境における長半減期核種の長期的化学挙動に関する次の研究である。

1）水に晒されたガラスの変質層についての鉱物学的研究を研究室での実験及び天然のガラスの調査により実施した。また，Ｐｕ及びＮｐの浸出実験を実施した。

2）放射性核種の固定に関する長期的反応過程のモデル化の研究のために分光学的手法を適用し，天然物を使って研究した。

東海研究所：〒319－11 茨城県那珂郡東海村白方字白根２－４

Contents

目　　次

Introduction

H. Nakamura

The pilot plant for the vitrification of high-level waste (HLW) is constructed by the Power Reactor and Nuclear Fuel Development Corporation (PNC) and the specifications of returnable waste from oversea reprocessing were endorsed by the government. The specifications of the glass waste form and the storage facility can be discussed realistically. On the other hand, the development of geological disposal has not progressed significantly.

Necessity of fundamental researches to support the system performance of geological disposal are emphasized in related governmental meetings especially on long-term assessment. The studies of our group were concentrated to estimate the long-term chemical behaviors of radioactive nuclides in geological disposal system. As a problem updated, source term of air contamination at an accident of transportation and storage was studied to suport the governmental safety examination.

This report summarizes the status and results of studies performed in the fiscal year 1988 in the High Level Radioactive Waste Management Laboratory and the WASTEF (Waste Safety Testing Facility) Operation Division of the Department of Environmental Safety Research, JAERI. The relative annual reports have been previously published in the following numbers; JAERI-M 82-145, 83-076, 84-133, 85-090, 86-131, 87-131 and 88-201.

1. Studies on waste forms

S. Muraoka

Studies on waste forms have been carried out to obtain source term data useful for safety evaluations of the waste management techniques on glass forms and to develop a new technology on Synroc.

Volatilization behaviors of radioactive substances from glass forms were investigated as a safety assessment study relating the interim storage.

For the long-term evaluation of geological disposal, leachability has been studied on glass forms containing various radionuclides such as Pu and Np. By using the natural glass the altered surface layer was investigated mineralogically as a validation study of long-term durability of glass forms.

Radiation stability of glass forms and Synroc has been studied using a ^{244}Cm doping method for evaluation over 10000 years equivalent.

1.1 Studies on leaching and volatilization of radionuclides from glass waste form

(1) Continuous-flow leach tests of simulated high-level waste glass in synthetic basalt groundwater

H. Kamizono

The present study aims at examining the leaching behavior of the HLW glass under reproducible laboratory conditions which simulate actual disposal situations as closely as possible. For instance, one type of synthetic groundwater, the composition of which is similar to Grande Ronde basalt groundwater, is used as leachant. The MCC-4 continuous-flow leach test method is adopted, since this method was developed for dynamic testing and has the possibility of being widely accepted as a standard method. Linear flow rates of the leachant are adjusted to values of less than 0.55 cm/d as such rates are believed to occur in geologic disposal sites. From this point, the experimental scheme is divided in three phases.

Phase 1: Simulated HLW glass is used without gamma irradiation.

Phase 2: Simulated HLW glass will be used with gamma irradiation.

Phase 3: Actual HLW glass will be used.

As of now, the phase 1 experiments have been completed and their results are described here as reference data for future comparison with those from phases 2 and 3.

The continuous flow leach tests were carried out at 90°C ± 1°C for up to 180 d using an MCC-4 type leaching apparatus. The leachant stored in the reservoirs was pumped into the leach containers through peristaltic pumps at fixed linear flow rates of 0.00055 to 0.55 cm/d. The leachant then made contact with the specimens which were held on supports, was moved away by periodic siphonic motions and stored in receiver bottles. The whole leachate from one outlet for about 20 d was stored in one receiver bottle and re-stored in a different bottle for leachate analyses.

The apparatus was further improved in four ways as follows:

(i) The shape of the leach containers was designed to provide three glass-surface-area to leachant-volume ratios of 10, 1 and 0.1 cm^{-1}. These required fifty pineapple-sliced specimens, five pineapple-sliced specimens, and one discoid specimen, respectively. When the pineapple-sliced specimens were placed in one leach container, the

distance between each specimen was 0.15 cm.

(ii) The leach containers and the connected leachant-inlets and outlets were made of stainless steel capable of enduring gamma irradiation of about 1 MGy, which would be one possible experimental condition in our future work.

(iii) The movable parts of the apparatus, such as the receiver bottles, which had to be handled throughout the experiments, were designed to be easily manipulated in a hot cell so that leach tests could be operated under a high gamma irradiation field.

(iv) All outlets were covered with heaters to maintain their temperature at about 90°C in order to prevent any re-precipitation of elements dissolved in the leachates while being transported to the receiver bottles.

Figure 1 shows an example of the relationship between the normalized concentration (NC) of each element and the time in days. Note that the difference between NC_B and NC_{Si} widens remarkably for the first 20 d, and narrows thereafter.

Since boron is a component in the network structure of the glass and the hydration of boron may initiate the degradation of the glass [1], the hydration of boron may dominantly control the kinetics of the glass dissolution at least at the beginning of leaching. After a relatively short period of leaching, silicon approaches its saturation concentration and then dissolved silicon starts to suppress further dissolution of the glass, which results in the formation of a silicon-rich surface layer on the glass. The hydration of boron matches the extent of the dissolution of silicon after the formation of the silicon-rich surface layer. The process of leaching described above is the best speculation, and further study is necessary to confirm the role of boron in the leaching of HLW glass.

Since the normalized concentrations of molybdenum, cesium and strontium are nearly constant throughout the 180-d duration, the formation of materials which have low solubility is expected. The observation and identification of such materials will also be undertaken in our future study.

Reference

1. Zhu B.-F. Nuclear waste glass leaching in a simulated granite repository. Doctor Thesis, University of Florida, Gainesville, Florida (1987).

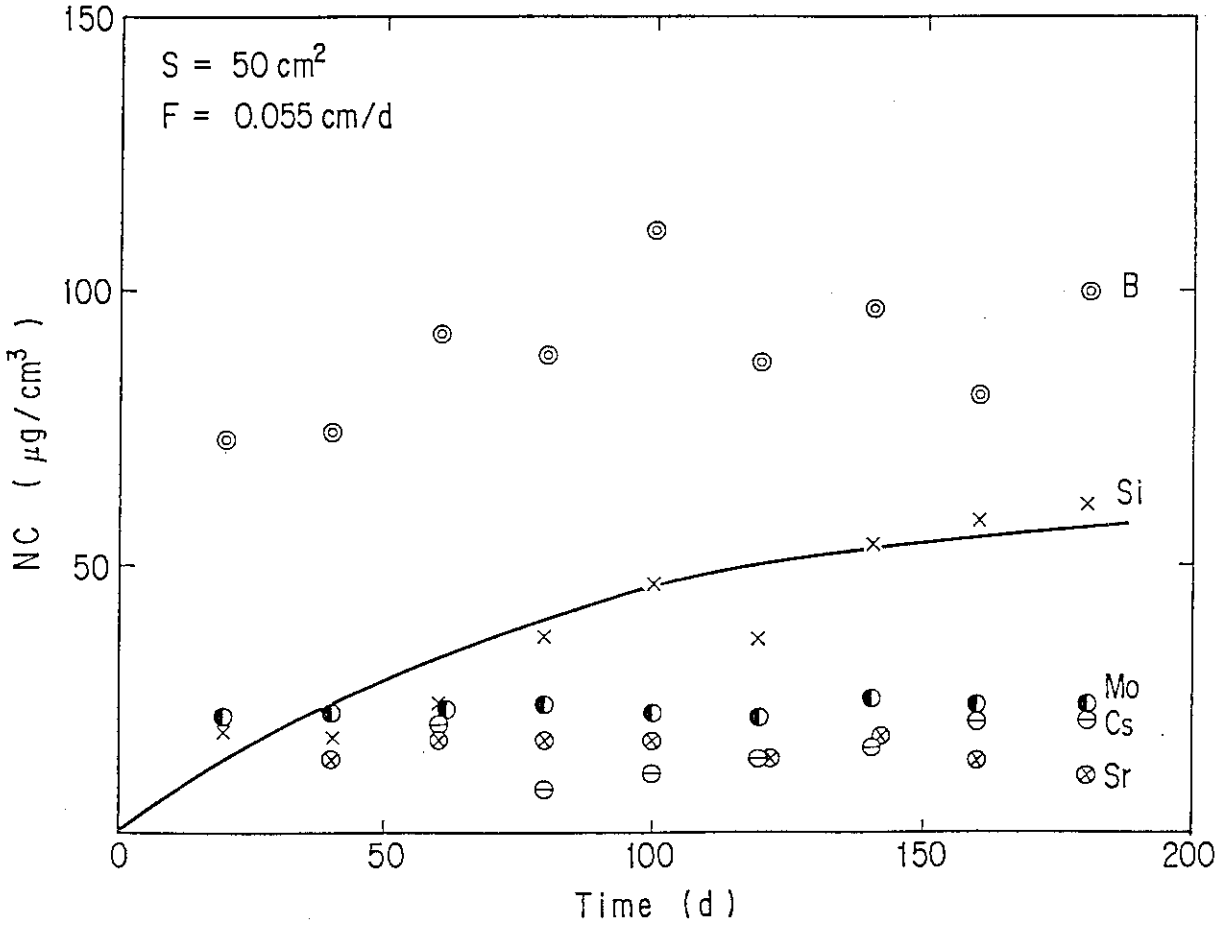

Fig. 1 Relationship between the normalized concentrations of various elements in the leachates and the time in days.

(2) Formation and evolution of alteration layers of borosilicate and basaltic glasses I: Initial stage

T. Murakami and T. Banba

Long-term (up to 10^7 years) leach rates of borosilicate glass can be predicted through a geochemical model. The more the model is required to be precise, the more we need a combined study of synthetic, borosilicate glasses and natural, basaltic glasses; the formers include information on leachant but not on time more than ten years while the latters include information on time up to tens of millions of years but not on leachant. Analytical electron microscopy (AEM) study was made on a synthetic, borosilicate glass and natural, basaltic glass to examine formation and evolution of the crystalline and non-crystalline phases in alteration leach layers of the two different glasses.

MCC-1 type experiment was carried out for the borosilicate glass (48.49 SiO_2, 11.30 Na_2O, 18.58 B_2O_3, 1.87 CaO, 2.00 Al_2O_3, 3.55 Fe_2O_3, 1.87 Li_2O, 2.87 ZrO_2, 0.34 SrO, 1.74 MoO_3, 0.26 MnO_2, 0.12 CoO, 0.33 NiO, 0.98 Cs_2O, 0.51 La_2O_3, 1.42 CeO, 1.65 Nd_2O_3 by wt%; other simulated waste elements are also contained) in deionized water at 90°C. The basaltic glass (51.1 SiO_2, 15.4 Al_2O_3, 11.1 FeO, 3.3 Na_2O, 6.3 MgO, 9.2 CaO, 1.8 TiO_2, and 0.2 MnO_2 by wt%), A5B, is form Ash Mountain, British Columbia, and formed in late Pleistocene (about 10,000 years ago) and reacted with meteoric water. Three- and fourteen-day leached samples (90-3 and 90-14, respectively) of the borosilicate glass were impregnanted by epoxy resin and ultramicrotomed for the AEM observations along with A5B. Leach solutions of the borosilicate glass were analyzed for up to 91 days.

90-14. The layer is 8μm in thickness and single-layered but not multi- or mixed-layered. The texture changes gradually from the glass side to the solution side; electron amorphous phases in mottled texture is dominant in the first half of the layer (near the glass), and in the second half of the layer (near the solution) fibers are scattered in the amorphous matrix. The nearer the fibers are located to the solution side, the more in number and the more developed they are. The size of the fibers is mostly less than 20 nm in length and 5 nm in thickness. The surface of the layer is covered with well-

developed fibers (less than 150 × 15 nm). The lattice fringes of the fibers have 0.7-, 1.0-, 1.2-, and 1.4-nm d-spacings which are usually irregularly interstratified. Analyses of the fibers (e.g., $Na_{0.61}(Al_{0.20}Fe_{1.16}Co_{0.36}Ni_{0.97}Mn_{0.01}Mo_{0.04})(Si_{3.53}Al_{0.47})O_{10}(OH)_2$ for F of 90-14 in Table 1) and the four kinds of d-spacings reveal that the fibers are a mixture of smectite (possibly Ni-rich nontronite) and chlorite (or septechlorite). The change of compositions in the layer is given in Table 1. The fibers do not contain Zr or rare earth elements although these elements remarkably increase in their contents as analytical points move from the glass side to the solution side. In contrast with Zr and rare earth elements, Co and Ni show no significant changes in the layer but greater amounts of Co and Ni are contained in the fibers than their initial amounts in the as-prepared glass. Fe content increases continuously from the glass side to the solution side and a large amount of Fe is contained in the fibers. This, along with the fact that the fibers grow out of amorphous-constitutent hydroxides, implies that Fe is a key element for the growth of the fibers.

90-3. Although the layer is thin (800 nm), it is essentially same as the 90-14 layer in terms of texture, composition, and mineralogy. Fibers are much less found and poorly-developed in the layer and on the surface of the layer. They have a few unit-layers along the c axis. The compositions of the fibers are similar to those of the 90-14 layers (Table 1).

A5B. The layer of the A5B glass varies its thickness considerably. One of the thickest part of the layer (600 μm) was used for the present study. The layer consists of alternating sublayers of an amorphous, fiber-free part and fiber-bearing part. Each part has a thickness of around 1 μm. The fibers are also scattered on the surface of the layer like those of the 90-3 layer. The fibers are a mixture of smectite and chlorite (1.0-, 1.2-, and 1.4-nm d-spacings) like the borosilicate glass layers. An example of the fiber analysis is given as $Na_{0.19}(Al_{0.76}Fe_{2.24}Mg_{0.04}Ti_{0.17})(Si_{2.44}Al_{1.56})O_{10}(OH)_2$ (F-2 of A5B in Table 1). Large crystals (10-50 × 50-100 nm) of smectite form usually at the interface of the two different sublayers.

Formation and evolution of the leach layers at the early stage are; amorphous phases (possibly metal hydroxides) form first and then

fibers of smectite and chlorite grow in the amorphous matrix and especially on the surface of the layer. The fibers are poorer in Si, and richer in Al, and much richer in Fe than the matrix. The changes in contents of elements in the layer and the movement of elements between phases during the formation and evolution are very important when radionuclide release from a borosilicate glass lasts over a long geologic period. This study demonstrated that, if leach layers of natural, basaltic glass are selected properly, they can be a good natural analogue to those of borosilicate glass in terms of the formation and evolution of crystalline and non-crystalline phases in the layers. Because rare earth elements are not contained in the fibers and not detected in the solutions, it is an important subject in the future how they remain in the layer.

Table 1 Compositions of selected areas in the layers

	Na_2O	MgO	Al_2O_3	SiO_2	ZrO_2	CaO	TiO_2	MnO_2	FeO	CoO	NiO	REO[a]
90-14												
GL	14.5	-	2.6	62.4	3.7	2.4	-	0.3	4.6[b]	0.2	0.4	4.6
G-1	7.6	-	10.3	62.3	6.6	1.1	-	0.2	5.2	0	0	4.2
G-2	3.6	-	7.8	55.6	10.4	1.1	-	0.8	8.6	0.1	0	8.9
S-1	3.7	-	4.8	48.2	13.5	0.9	-	1.0	10.9	0.2	0.4	11.3
S-2	3.2	-	4.6	49.4	15.2	0.7	-	1.3	11.0	0.2	0.4	11.8
F	4.0	-	7.3	45.6	0	0	-	2.8	17.8	5.8	15.6	0
90-3												
G	3.6	-	7.9	57.7	12.2	0.9	-	0.6	6.5	0.3	0.7	5.2
S	3.3	-	2.7	47.1	11.5	0	-	2.1	15.5	0	0.6	15.1
F	1.7	-	13.3	42.8	0	0	-	1.0	17.7	6.8	16.1	0
A5B												
A-F	1.0	0.4	36.3	43.0	-	0	3.1	-	16.0	-	-	-
A-B	0.9	1.0	43.5	40.3	-	0.2	2.4	-	11.5	-	-	-
F-1	0.4	0	38.2	30.9	-	0	4.0	-	26.4	-	-	-
F-2	1.3	0.4	26.5	32.8	-	0	3.0	-	36.0	-	-	-

[a] sum of La_2O_3, CeO, and Nd_2O_3; [b] value as Fe_2O_3; GL is a composition of as-prepared borosilicate glass recalculated excluding B_2O_3 and Li_2O; G and S represents areas near the glass side and the solution side, respectively, and the lager the number after the letter G or S, the nearer the analytical area is to the solution side; F represents fibers; A-F and A-B denote a fiber-free amorphous part and a fiber-bearing amorphous part, respectively.

(3) Growth rate of alteration layer and elemental mass losses during leaching of borosilicate waste glass

T. Banba and T. Murakami

In order to validate the predictive models of the long-term corrosion of nuclear waste forms, the concept of natural analogues has been proposed[1]. The problem is, however, how we utilize the information of the natural analogues for modelling. One of the ways is to justify confidence in the theoretical model by correctly predicting the phases formed in the alteration layers of naturally and experimentally altered glasses. That is why a detailed understanding of the mineralogy and geochemistry of the layers is required[2]. In the present paper, we will discuss on the growth rate of the alteration layer of a borosilicate nuclear waste glass and the relevance to elemental mass losses.

MCC-1 static leaching experiments were carried out for a borosilicate waste glass in deionized water for up to 364 days at 90°C. Four plate samples were put in a container for each leaching interval. One of the four was immersed in ethanol for 2 hours just after removing it from leachate in order to avoid the shrinkage of the alteration layers during drying. The others were air-dried. Low viscosity epoxy resin was poured on the ethanol-immersed sample just after ethanol was discarded. It was preliminary confirmed that the resin is soluble in ethanol. The air-dried samples were vacuum impregnated in the resin. After polymerization of the resin, the samples were cut perpendicular to the original glass surface and polished. The sections were subjected to optical microscopy (OM). In the case that the layers were too thin for OM, the samples were cut by ultramicrotome and then subjected to analytical electron microscopy (AEM). Elemental concentration of the leachates were analyzed by means of inductively coupled plasma atomic emission spectroscopy (ICP-AES) or atomic absorption spectrometry (AAS).

The thickness of the alteration layers increased linearly at a rate of 0.63 μm/day for up to 91 days. After 91 days, however, the thickness was kept constant (about 60 μm), independent of time. This implies that significant corrosion of the glass would cease after 91-day leaching, and consequently, the reaction between the alteration layers and the leachate would play a major role in the corrosion.

The above implication is supported by the AEM observation that the structure of the alteration layers changes with time[2].

The apparent release of Si and B ceased after 91-day leaching as well as the thickness of alteration layers, and their time dependence curves were similar to that of the layer thickness. Both elements are probably associated with the layer thickness. The depletion of B in the alteration layers has been confirmed by the SIMS depth profiles of leached glasses reported by many workers (see, for example, ref.3). Therefore, we assumed that B was completely depleted from the alteration layers, so that the layer thickness was calculated based on the amount of B in leachates. These calculated values of layer thickness, represented by the triangles in Fig. 1, agreed well with the observed values by OM or AEM measurements. This suggests that the alteration layer thickness can be estimated by the amount of B released. The agreement also implies that shrinkage of the alteration layers is not significant, and that the alteration layers retain their framework even after the depletion of part of the glass network formers and the recrystallization which has been reported previously[2]. The retention of the layer framework is, however, inconsistent with the fact that the naturally altered layer of basaltic glass of about a million years in age has voids and interstices, and is highly crystallized[4].

By comparison of the ethanol-immersed samples with the air-dried ones, it was found that the air-dried layers were thinner by 5 percent after 91-day leaching, and that the variability of the thickness of the air-dried layers was larger (Figure 1). This is because shrinkage of the layers occurred in the air-dried samples during air-drying. Naturally altered basaltic glasses are usually obtained as dried ones. Therefore the structural change of alteration layers during air-drying should be understood, of which the investigation is in progress.

References

1. R.C. Ewing and M.J. Jercinovic, MRS Symp. Proc. Vol.84, 67 (1987).
2. T. Murakami, et al., MRS Symp. Proc. (in press) (1989).
3. Zhihong Zhou and W.S. Fyfe, MRS Symp. Proc. Vol.112, 725 (1988).
4. T. Murakami, M.J. Jercinovic, and R.C. Ewing, in preparation.

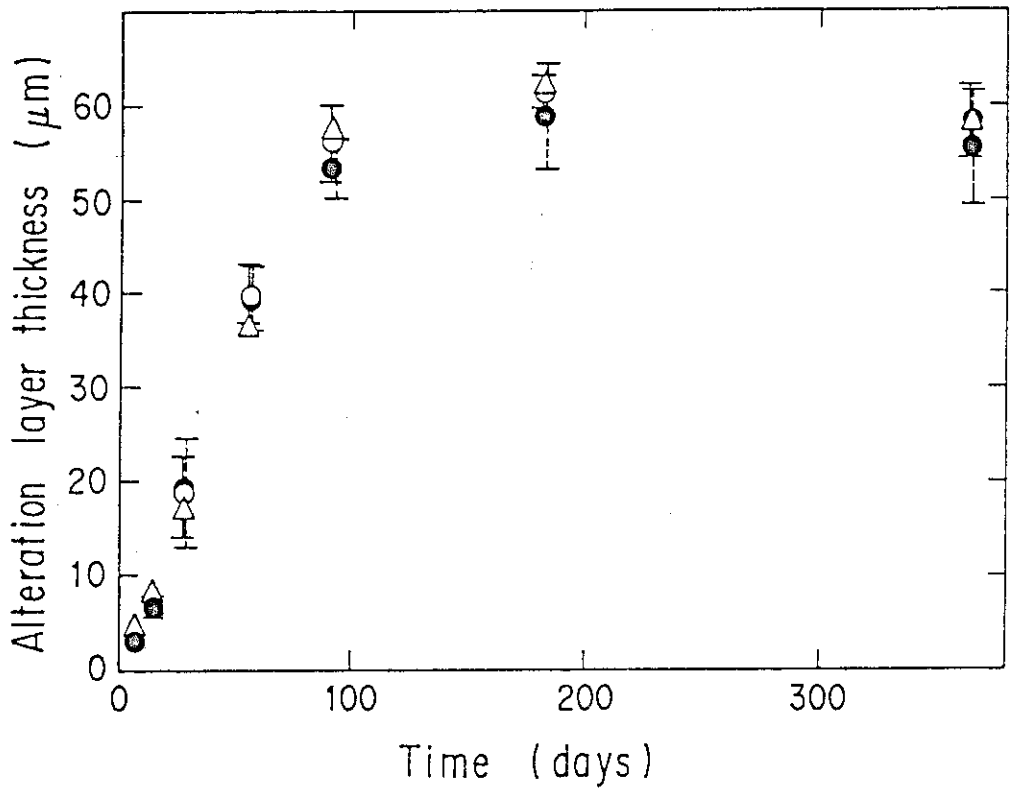

Fig. 1 Graph of the thickness of alteration layers as a function of leaching time under MCC-1 condition at 90°C. The open and solid circles indicate the averages in the thickness of the ethanol-immersed and air-dried layers, respectively. The error bars represent the variability in the layer thickness. The triangles indicate the layer thickness calculated from the amount of B release in leachates.

1.2 Leaching of Pu and Np

(1) Temperature effect on Pu leach rate of the nuclear waste glass

T. Banba

INTRODUCTION

The leachability of nuclear waste glasses has been investigated intensively for the reason that a waste form is the first barrier material from the release of radionuclides in the repository. Recently, the investigations on the leaching behavior of actinide elements from various approaches are being carried out, since actinides with long half-lives have the potential of long-term environmental hazards. Several researchers have pointed out that the solubilities of actinides play a significant role in the actinide releases from the waste glass[1][2][3]. Whereas, the solubilities should be due to the chemical forms of actinides in the bulk glass or in the leached surface layer. Concerning Pu, Apted and coworkers have predicted that the dissolution of hydrated, amorphous compounds formed in the leached surface layer rather than simple oxide in the bulk glass controls the release rate of Pu[1].

In the present paper, the dissolution kinetics of the plutonium compounds in the surface layer is examined by the comparison between the temperature dependence of initial leach rates of Pu and that of other elements contained in the waste glass.

EXPERIMENTAL

Preparation of waste glasses

Two kinds of waste glasses with a similar composition were prepared, separately. The non-radioactive simulated waste glass, which was melted in a platinum crucible at 1150°C for two hours, was annealed at 550°C for one hour in a graphite mold and slowly cooled down to room temperature. The ^{238}Pu-doped glass was prepared using the mixture of powdered simulated waste glass and plutonium oxide ($^{238}PuO_2$) in a platinum crucible of 14 mm in diameter under the same heating conditions as above. The content of PuO_2 was 1.35 wt% (^{238}Pu: 6.6×10^9 Bq/g-glass). The compositions of both waste glasses are shown in Table 1. The test specimens (14 mm^{ϕ} × 8 mm^{t}) of both glasses were prepared by cutting and polishing.

Leach test method

ISO type leach tests[4] were carried out in distilled water. The leach containers of Teflon were used for all tests. The ratio of surface area to leachant volume (SA/V) was 0.1 cm^{-1}. Tests were conducted at temperatures between 23°C and 90°C for up to 64 days. A single specimen of non-radioactive simulated waste glass and five separate specimens of ^{238}Pu-doped glass were independently immersed in leachant at each test temperature. These specimens were cleaned by ultrasonic washing with ethyl-alcohol for 10 min, and dried at 110°C for one hour. After predetermined intervals each specimen was withdrawn from the leach container and immediately transferred to a new leach container filled with fresh leachant. Solution analyses were carried out for the leachates of non-radioactive simulated waste glass using the inductively coupled plasma spectroscopy (ICP) and the atomic absorption spectroscopy (AAS). Plutonium-238 concentrations were determined through a combination of gas flow proportional counting and surface barrier spectrometry techniques.

The pH of leachate was measured with a pH meter of TOA Electronics Ltd, Model HM-10K.

Results and discussion

In the case of short-term leaching, in which the protective effect of the leached surface layer is neglected, the dissolution of the glasses in aqueous solution can be described as a reaction of first order, as shown by Rimstidt and Barnes[5]:

$$SiO_2(s) + 2H_2O(l) = H_4SiO_4(aq). \quad (1)$$

Assuming this first order reaction, the dissolution rate r(t) is:

$$r(t) = \frac{V}{SA} \cdot \frac{dc_{Si}}{dt} = k(c_{Si,sat} - c_{Si}) \quad (2)$$

where V is the volume of solution [m^3], SA is the surface area of specimen [m^2], c_{Si} is the concentration of Si in solution [g/m^3], t is the time [sec], k is the rate constant [m/sec], and $c_{Si,sat}$ is the saturated concentration of Si in solution [g/m^3]. In the case of $c_{Si} \ll c_{Si,sat}$, Eq.(3) is obtained from Eq.(2) and the normalized elemental mass loss of Si, $NL_{Si} = c_{Si} \cdot V \cdot MG/(SA \cdot MG_{Si})$, where MG and MG_{Si} are the mass of glass specimen and the atomic mass of Si in the specimen,

respectively.

$$\frac{d(NL_{Si})}{dt} = k \cdot c_{Si,sat} \frac{MG}{MG_{Si}} \tag{3}$$

The integrated form of Eq.(3) is

$$NL_{Si} = k \cdot c_{Si,sat} \frac{MG}{MG_{Si}} t = k't \tag{4}$$

where $k' = k \cdot c_{Si,sat} MG/MG_{Si}$ [g/(m^{2}sec)].

If the equation (4) is applied to the present leaching data, the rate constant k' can be obtained in term of g/(m^{2}day) and their temperature dependency can be calculated. Figure 1 shows the normalized elemental mass loss of Si, NL_{Si}, in the initial stages of the ISO-test as a function of time at 23, 45 and 70°C. From the initial positive slopes of the curves in Fig. 1, which are uninfluenced by the saturation effect, the rate constant k' at each temperature can be determined for the leaching process. The normalized mass losses of the other elements in the initial stages of leaching are also represented by the equation (4) as shown in Fig. 2 and Fig. 3. Therefore, the rate constants of the initial release of each element at each temperature can be determined in a similar manner as above.

Figure 4 shows the rate constants k' of Si, Na, Sr, Cs and Pu as a function of reciprocal temperature. The rate constants of four elements except Pu, can be adequately approximated by one straight line, so that an activation energy can be determined according to the Arrhenius relation: $k' = A \cdot \exp(-E_a/RT)$, where A is the frequency factor, E_a represents the activation energy [kJ/mol], R represents the gas constant [8.314 J/(mole K)], and T is the temperature [K]. Its value was 78±9 kJ/mol, which agreed with the activation energies of around 60 to 80 kJ/mol previously observed in the nonsaturating case[6]. This result implies that Na, Sr and Cs are released from the waste glass with the same mechanisms as the dissolution of the glass matrix in the initial stages of leaching, and that the effect of the leached surface layer on the initial leach rate of these elements can be neglected.

On the other hand, an activation energy obtained for Pu is 22±10 kJ/mol, which is much lower than the above activation energy of dissolution of glass matrix. This means that the release of Pu is not

controlled by the glass matrix dissolution even in the initial stages of leaching. Based on the comparison between Pu concentration in solution and solubility of hydrous plutonium dioxide, $PuO_2 \cdot xH_2O$, Apted et al. have predicted that the amount of Pu released from the glass is controlled by the formation of amorphous $PuO_2 \cdot xH_2O$ on the glass surface during the leach test[1]. If the amorphous $PuO_2 \cdot xH_2O$ is formed in the leached surface layer, and its formation rate is much faster than the dissolution rate, the release of Pu should be controlled by the following reaction.

$$PuO_2 \cdot xH_2O \rightarrow Pu^{4+} + 4OH^- + (x-2)H_2O \qquad (5)$$

This reaction is also supported by the results reported by Rees and coworkers. That is, at 25°C and 90°C, a significant Pu^{4+} concentration of the leachates in the initial stages of leaching was measured[7]. Therefore, the activation energy obtained in the present experiments is suggested to be the activation energy of the reaction (5). Up to data, no experimental data on the temperature dependence of rate constants for this reaction can be found.

References

1. Apted, M.J., McVay, G.L. and Wald, J.W.: Release of actinides from defense waste glass under simulated repository conditions, Nucl. Technol., 73, 165 (1986).
2. Rai, D. and Ryan, J.L.: Solubility constraint: An important consideration in safety assessment of nuclear waste disposal, "Mat. Res. Soc. Symp. Proc.," Vol.26, (McVay, G.L., Ed.), p.805 (1984).
3. Kim, J.I., Treiber, W., Lierse, C. and Offerman, P.: Solubility and colloid generation of plutonium from leaching of a HLW glass in salt solutions, "Mat. Res. Soc. Symp. Proc.," Vol.44, (Jantzen, C.M. et al., Eds.), p.359 (1985).
4. "Long-term Leach Testing of Radioactive Waste Solidification Products," ISO/DIS-6961, International Organization for standardization (1979).
5. Rimstidt, J.D. and Barnes, H.L.: The kinetics of silica-water reactions, Geochim. Cosmochim. Acta, 44, 1683 (1980).
6. Barkatt, A., Simmons, J.H. and Macedo, P.B.: Corrosion mechanisms and chemical durability of glass media proposed for the fixation

of radioactive wastes, Nucl. Chem. Waste Manag., 2, 3 (1981).

7. Rees, T.F., Cleveland, J.M. and Nash, K.L.: Leaching of plutonium from a radioactive waste glass by eight groundwaters from the western United States, Nucl. Technol., 70, 133 (1985).

Table 1 Composition of Simulated High-Level Waste Glasses

Component	Content (wt%) Non-doped Glass*	Content (wt%) ^{238}Pu-doped Glass	Component	Content (wt%) Non-doped Glass*	Content (wt%) ^{238}Pu-doped Glass
Additive			Waste		
SiO_2	45.15	45.15	TeO_2	0.23	0.23
B_2O_3	13.90	13.90	Cs_2O	0.98	0.98
Al_2O_3	4.89	4.89	BaO	0.62	0.62
CaO	4.00	4.00	La_2O_3	0.50	0.45
Na_2O	9.79	9.79	CeO_2	1.91**	0.90
ZnO	2.47	2.47	Pr_6O_{11}	0.49	0.44
Li_2O	2.00	2.00	Nd_2O_3	1.65	1.48
			Sm_2O_3	0.32	0.29
Waste			Eu_2O_3	0.06	0.05
Rb_2O	0.12	0.12	Gd_2O_3	0.04	0.03
SrO	0.34	0.34	SeO_2	0.02	0.02
Y_2O_3	0.20	0.18	RuO_2	0.80	0.80
ZrO_2	2.64	2.64	Fe_2O_3	2.90	2.90
MoO_3	1.73	1.73	NiO	0.40	0.40
MnO_2	0.26	0.26	Cr_2O_3	0.50	0.50
Ag_2O	0.03	0.03	P_2O_5	0.30	0.30
CdO	0.03	0.03	Ru	0.12	0.12
SnO_2	0.02	0.02	Rh	0.15	0.15
Sb_2O_3	0.01	0.01	Pd	0.43	0.43
			PuO_2	-	1.35

* : This represents the non-radioactive simulated waste glass.
**: This value includes the total content of actinide oxides (0.9 wt%) simulated by CeO_2.

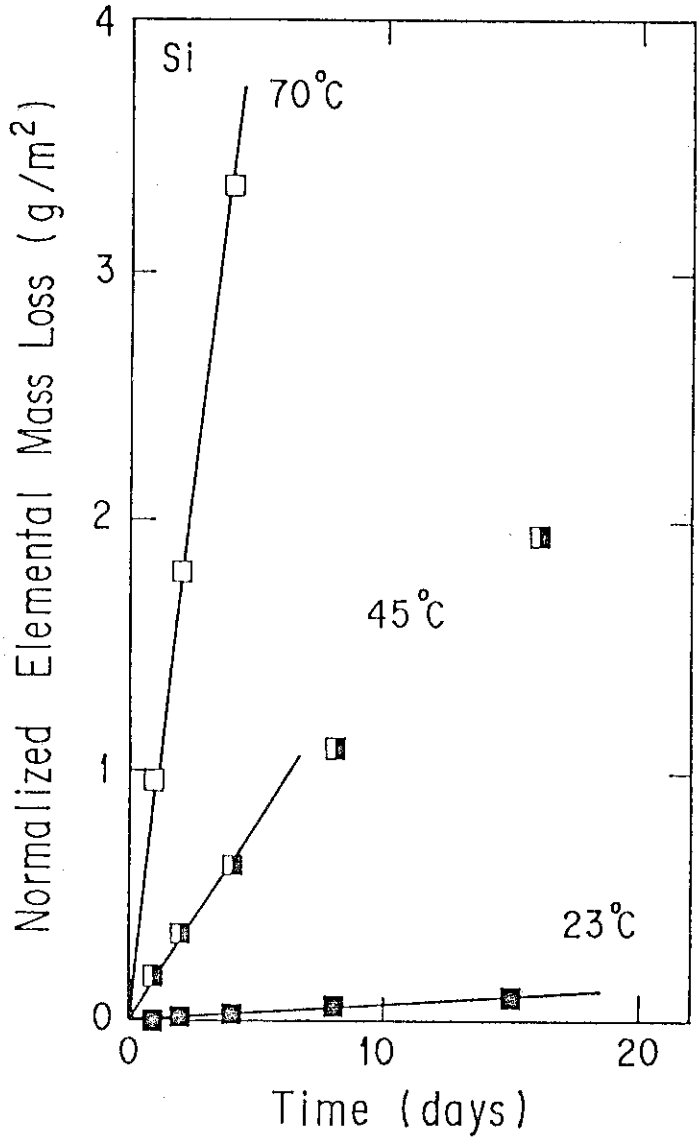

Fig. 1 The normalized elemental mass loss of Si in the initial stages of the ISO-test as a function of time at 23°C, 45°C and 70°C.

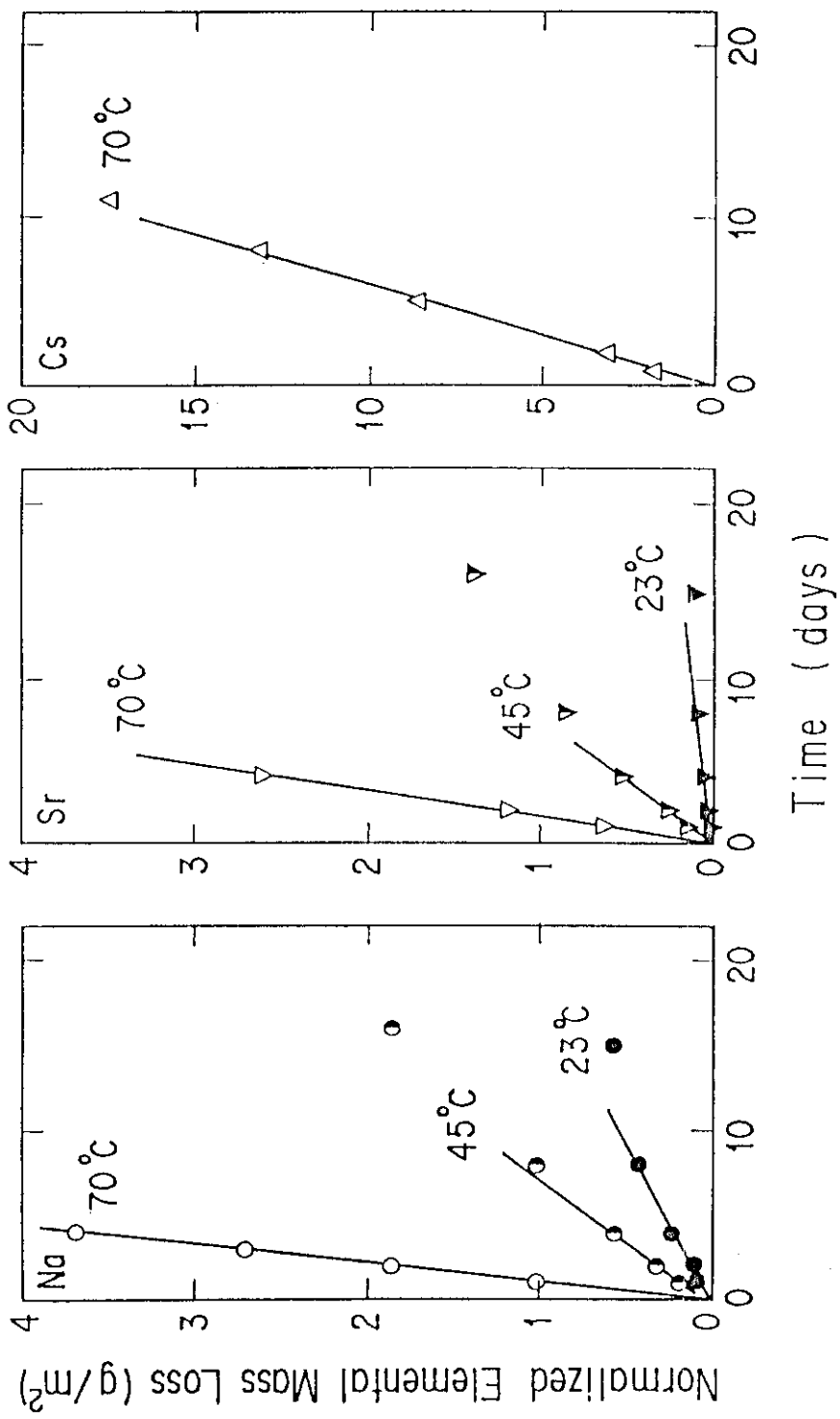

Fig. 2 The normalized elemental mass loss of Na, Sr and Cs in the initial stages of the ISO-test as a function of time at 23°C, 45°C and 70°C.

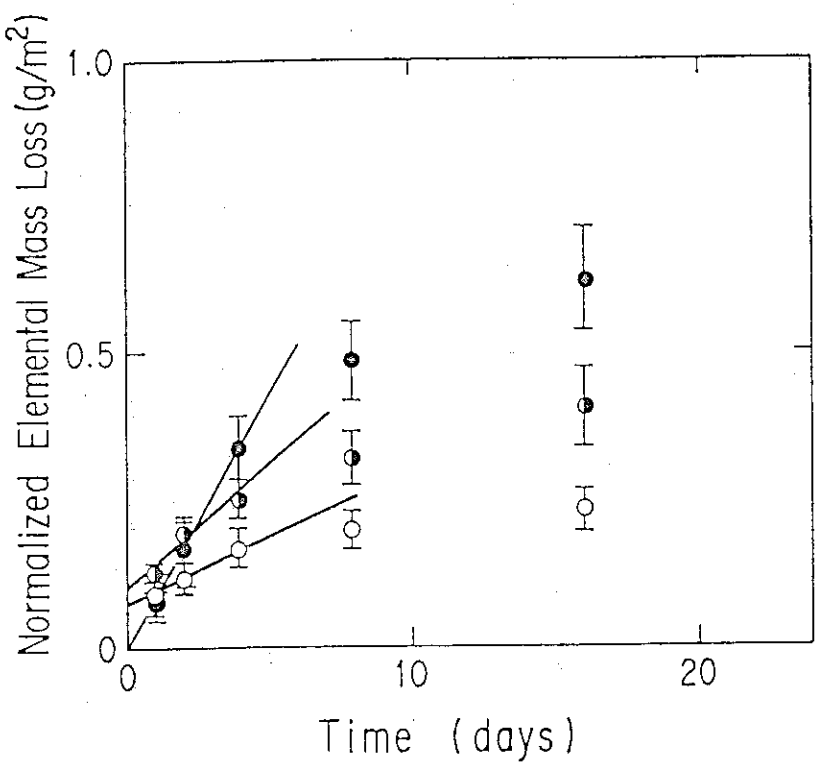

Fig. 3 The normalized elemental mass loss of ^{238}Pu in the initial stages of the ISO-test as a function of time at 25°C(○), 60°C(◑) and 90°C(●). Error bars show the standard deviations of each plot.

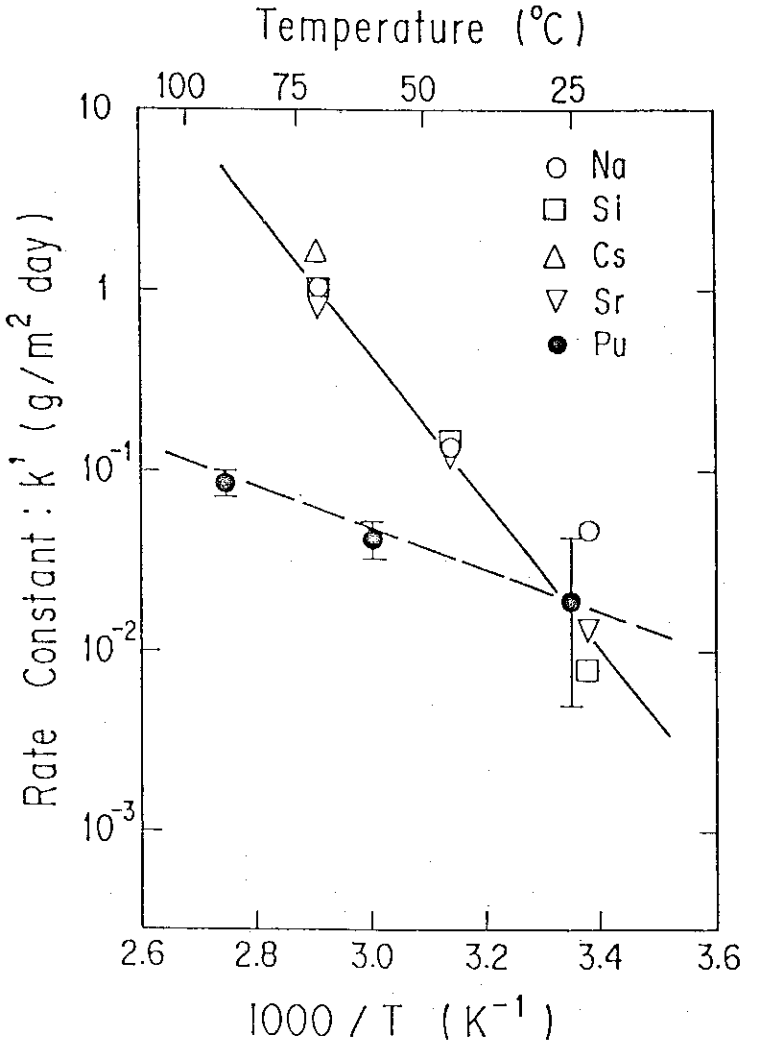

Fig. 4 The rate constants k' for the leaching process of the waste glass as a function of reciprocal temperature.

(2) Release of Np from Np-doped borosilicate waste glass

S. Nakayama and T. Banba

Introduction

The Materials Characterization Center (MCC) static leach tests[1] were performed for a neptunium-237 (^{237}Np)-doped borosilicate waste glass at 90°C with deionized water and silicate water leachants. We determined the concentrations of dissolved neptunium in the solutions contacting the ^{237}Np-doped glass in 3-day to 91-day leach tests. An attempt was made to estimate the release mechanism of neptunium from waste glasses.

Experimental

The composition of the Np-doped glass is shown in Table 1. The glass additives were referred to those of the R7T7 glass[2] and the waste composition to the JW-A.[3] Standard MCC-1 static leach tests[1] were performed at 90°C. Teflon® perfluoroalkoxy (PFA) vessels were used as leach containers. Before use these containers were cleaned enough to remove hydrofluoric acid to a negligibly low level[4]. About 30ml of leachant were added into a Teflon container, resulting in the SA/V ratio of 10 m^{-1}. Deionized water and silicate water[1] were used as leachants. At the desired leach durations, the neptunium concentrations in the leachates were determined by gamma-counting with a high-purity germanium detector.

The Teflon containers, after removing the glass specimens and the leachates, were washed with 30ml of 1 mol/l HNO_3 at 90°C for a day. The radioactivities in the HNO_3 solutions were indistinguishable from the background level, indicating negligibly small adsorption of neptunium on the vessel walls.

Results and Discussion

(i) Leachate Filtration

The ultrafiltration was applied to the leachates and particulate or polymeric neptunium species larger than 3 nm in size were not detected in both the deionized water and the silicate water leachates; neptunium released from the glass were in soluble species in both the leachates.

(ii) Release of Neptunium

The amounts of neptunium released from the studied glass are plotted as a function of time in Fig. 1 in terms of the normalized elemental mass loss $(NL)_{Np}$. Although the release behaviors as a function of time are appreciably different between the two leachates, the $(NL)_{Np}$ values of about 5 g/m^2 are similar for the two leachates after 91-day leaching.

The present results are comparable with the data reported in Refs. (5) to (8), considering the leaching conditions of the MCC-1-type leach tests at 90°C for monolithic glass specimens. The present $(NL)_{Np}$ values of about 5 g/m^2 are similar to most of the literature values, 1-10 g/m^2. It can be concluded that currently-studied, typical borosilicate waste glasses as well as the present glass have similar $(NL)_{Np}$ values of 1-10 g/m^2, meaning that they have similar ability to immobilize neptunium.

In Figure 2 comparison was made of the release behavior of neptunium obtained in this study with those of other elements from Ref.(9). A linear relation between log(NL) and log(time) is observed for sodium, boron and cesium within the studied leaching durations. As time proceeds, NL's for neptunium and strontium approach constant values while the linear relations are still held for sodium, boron and cesium. This fact implies the difference in the release mechanisms.

According to Banba and Murakami,[10] sodium, boron and cesium were found in the leachates but not found in the surface layer; they are released from the bulk glass by decomposition of the glass and diffuse through the surface layer without being trapped. Strontium was detected both in the surface layer and in the leachates. Probably neptunium, representing a similar time-dependent release behavior to that for strontium, was also present in surface layers.

(iii) Solubility Limits to the Neptunium Release

In a surface layer higher water content was observed than in a bulk glass,[11] meaning that a leachate entered the surface layer. It is therefore reasonable to assume that neptunium concentrations in glass leachates are controlled by the solubilities of neptunium soild phases formed in the surface layer. This assumption leads to that the solid phases formed in surface layers must be primarily identified in order to predict neptunium concentrations in glass leachates.

Since none of present analytical techniques is applicable to wet surfaces, the neptunium species in the surface layers can not be identified directly. Then, an attempt was made to estimate it based on the predicted species in the bulk glass and that in leachates. In bulk glasses either the tetravalent[12,13] or the pentavalent[14] species possibly exists. Neptunium species in aqueous solutions can be estimated by pH and Eh of the solutions. However, such redox parameters have not been studied for solutions contained in surface layers. Instead, we use pH and Eh values of the leachates. The measured pH and Eh of the leachates in the present experiments are plotted in Fig. 3. These values change with time, but they are similar for different leach durations of 7, 14, 28, 56, and 91 days. Referring to available pH-Eh diagrams,[15-17] the tetravalent and the pentavalent species are possibly present in comparable amounts in the present leachates, and the trivalent and the hexavalent species are probably absent. Since the tetravalent and/or the pentavalent species are expected to exist in both the bulk glasses and glass leachates, the valence of neptunium in the surface layer is also likely to be tetravalent and/or pentavalent.

Considering the above estimation on the valence and OH^- as a predominant complexing anion present in the glass leachates, we take $NpO_2 \cdot xH_2O$(am,am=amorphous) and NpO_2OH(am) as neptunium solid phases in the surface layer, and assume the following three types of solubility equilibrium; (1) $NpO_2OH(am)=NpO_2^+$, NpO_2OH(aq=aqueous), and $NpO_2CO_3^-$, (2) $NpO_2 \cdot xH_2O(am)=NpO_2^+$, (3) $NpO_2 \cdot xH_2O(am)=Np(OH)_4(aq)$. Other solid phases of neptunium than the above two were neglected because of the considerably low solubility product, or because of lack of data and/or their reliability.

Apparent steady-state concentrations of neptunium from MCC-1-type glass leach tests are plotted in Fig. 4. Predicted solubilities of NpO_2OH(am) and $NpO_2 \cdot xH_2O$(am) calculated from equilibrium constants at 25°C[18-25] are also shown in the same figure by dotted and hatched regions, respectively. These regions include the predicted solubilities for different ionic strengths of aqueous solutions. As seen in this figure, neptunium concentrations in the glass leach tests are apparently limited by the solubilities of $NpO_2 \cdot xH_2O$(am); the above-mentioned equilibria (2) and (3) are expected. Neptunium concentrations obtained from the glass leach tests are distinguishably lower

than the solubilities of NpO_2OH(am). If neptunium in the surface layers had been NpO_2OH(am), the neptunium concentrations in the leachates should have been higher, approaching the NpO_2OH(am) solubilities. These facts imply that neptunium exists as the tetravalent solid phase $NpO_2 \cdot xH_2O$(am) rather than the pentavalent solid phase NpO_2OH(am) in the surface layers of leached waste glasses.

References

1. Materials Characterization Center, Nuclear Waste Materials Handbook, DOE/TIC-11400, 1981.
2. Petit, J.-C., et al., "Scientific Basis for Nuclear Waste Management", Vol.12, in press.
3. Banba, T., et al., JAERI-M 82-088, 1982.
4. Nakayama, S., Banba, T., JAERI-M 88-201, (Nakamura, H., Tashiro, S. Ed.) 20, 1988.
5. Bates, J.K., et al., J. Mater. Res., 3, 576, 1988.
6. Bates, J.K., et al., "Scientific Basis for Nuclear Waste Management", Vol.6, (Brookins, D.G. Ed.) 183, 1983.
7. Apted, M.J., et al., Nucl. Technol., 73, 165, 1986.
8. McGrail, B.P., ibid., 75, 168, 1986.
9. Shimizu, I., Kamizono H., JAERI-M 86-070 (In Japanese, with English abstract, tables and figures.), 1986.
10. Banba, T., Murakami, T., Nucl. Technol., 70, 243, 1985.
11. Doremus, R.H., Nucl. Chem. Waste Manage., 2, 119, 1981.
12. Fahey, J.A., et al., J. Inorg. Nucl. Chem., 38, 495, 1976.
13. Eller, P.G., et al., Radiochimica Acta, 39, 17, 1985.
14. Veal, B.W., et al., CONF-860608--4, 1986.
15. Allard, B., et al., J. Inorg. Nucl. Chem., 42, 1015, 1980.
16. Inoue, Y., Tochiyama, O., Tech. Rep., Tohoku Univ., 47, 263, 1982.
17. Inoue, Y., Tochiyama, O., Bull. Chem. Soc. Jpn., 58, 588, 1985.
18. Rai, D., et al., Radiochimica Acta, 42, 35, 1987.
19. Maya, L., Inorg. Chem., 22, 2093, 1983.
20. Lierse, Ch., et al., Radiochimica Acta, 38, 27, 1985.
21. Kraus, K.A., Nelson, F., AECD-1864, 1948.
22. Sevostyanova, E.P., Khalturin, G.V., Soviet Radiochim. (Engl. Transl.) 18, 738, 1976.
23. Nakayama, S., et al., Radiochimica Acta, 44/45, 179, 1988.
24. Bidoglio, G., et al., ibid., 38, 21, 1985.

25. Moriyama, H., et al., In Symposium on Transuranium Elements Today and Tomorrow, Karlsruhe, October, 1988.
26. Allard, B., et al., Inorganica Chimica Acta, 94, 205, 1984.
27. Rai, D., et al., Nucl. Technol., 58, 69, 1982.
28. Bazan, F., et al., "Scientific Basis for Nuclear Waste Management", Vol.10, (Bates, J.K., Seefeldt, W.B. Ed.) 447, 1987.

Table 1 Composition of ^{237}Np-doped waste glass

Component	Content (wt %)	Component	Content (wt %)
Additive		Waste	
SiO_2	45.15	TeO_2	0.23
B_2O_3	13.90	Cs_2O	0.97
Al_2O_3	4.89	BaO	0.62
CaO	4.01	La_2O_3	0.48
Na_2O	9.79 *	CeO_2	0.95
ZnO	2.47	Pr_6O_{11}	0.46
Li_2O	2.00	Nd_2O_3	1.55
		Sm_2O_3	0.31
Waste		Eu_2O_3	0.06
Rb_2O	0.12	Gd_2O_3	0.03
SrO	0.34	SeO_2	0.02
Y_2O_3	0.19	RuO_2	0.80
ZrO_2	2.64	Fe_2O_3	2.90
MoO_3	1.73	NiO	0.40
MnO_2	0.26	Cr_2O_3	0.50
Ag_2O	0.03	P_2O_5	0.30
CdO	0.03	Ru	0.12
SnO_2	0.02	Rh	0.15
Sb_2O_3	0.004	Pd	0.43
		$^{237}NpO_2$	1.15

* : Component contains both additive and waste.

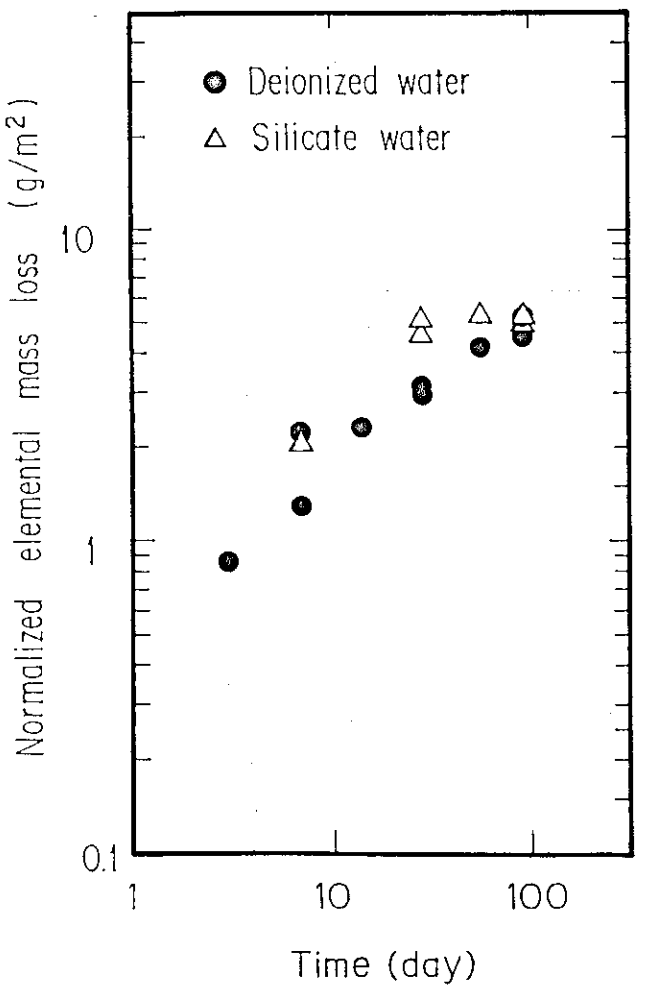

Fig. 1 The normalized elemental mass losses as a function of time for neptunium released from the ^{237}Np-doped borosilicate waste glass in the MCC-1 static leach tests at 90°C.

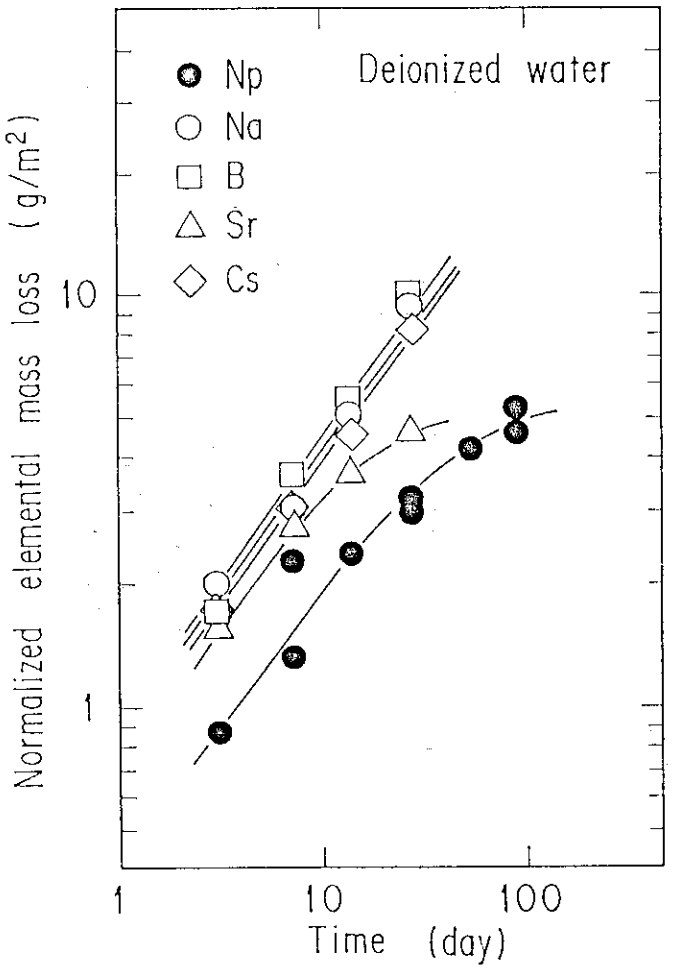

Fig. 2 The normalized elemental mass losses as a function of time for sodium, boron, strontium, cesium and neptunium released from JAERI glasses in the MCC-1 static leach tests. Data on neptunium in Fig. 1 for deionized water were replotted. Data on sodium, boron, strontium and cesium were cited from Ref.(9).

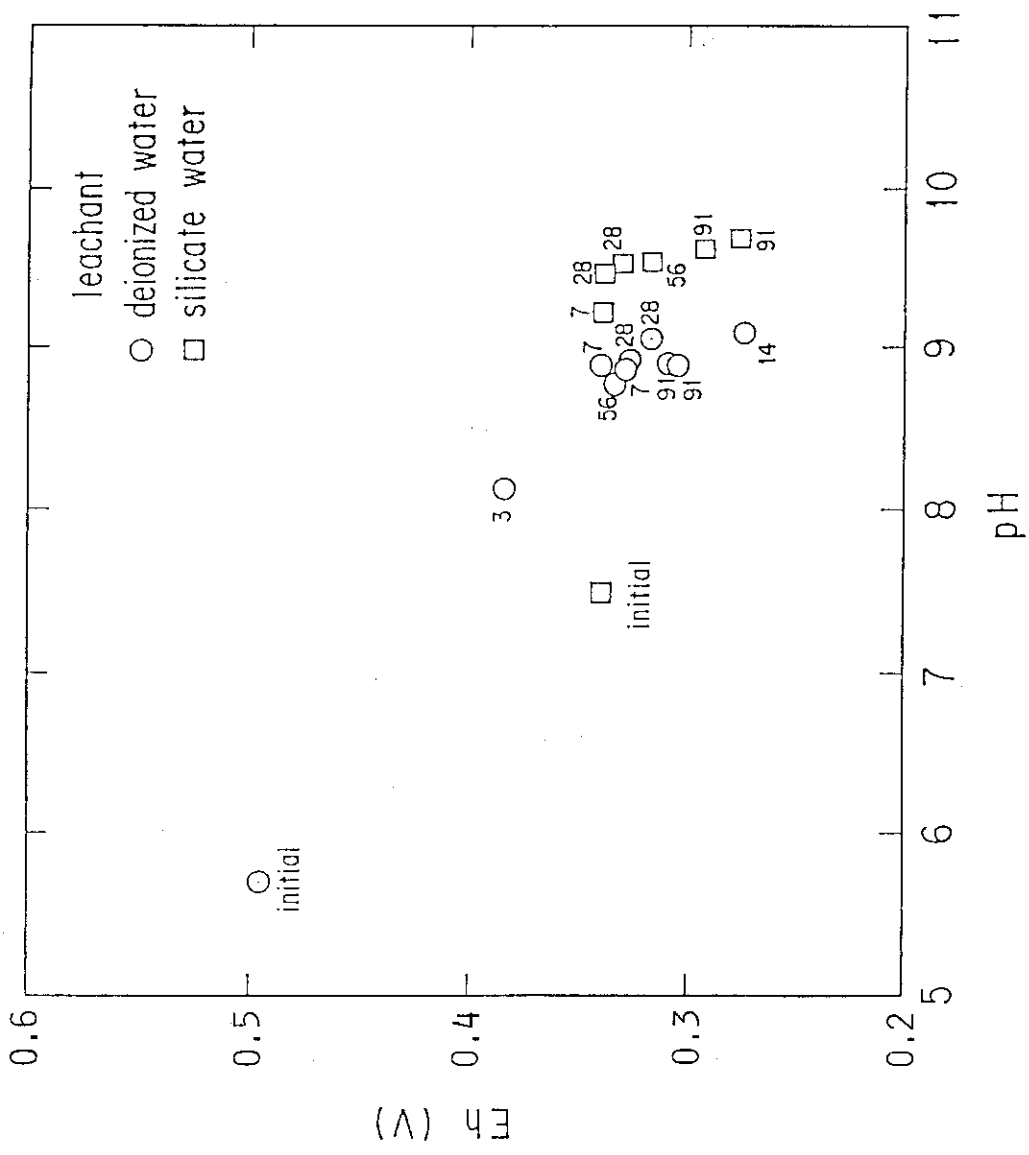

Fig. 3 Measured pH and Eh values of the glass leachates. Numbers next to the points denote the leach durations. The "initial"s denote the values for leachants.

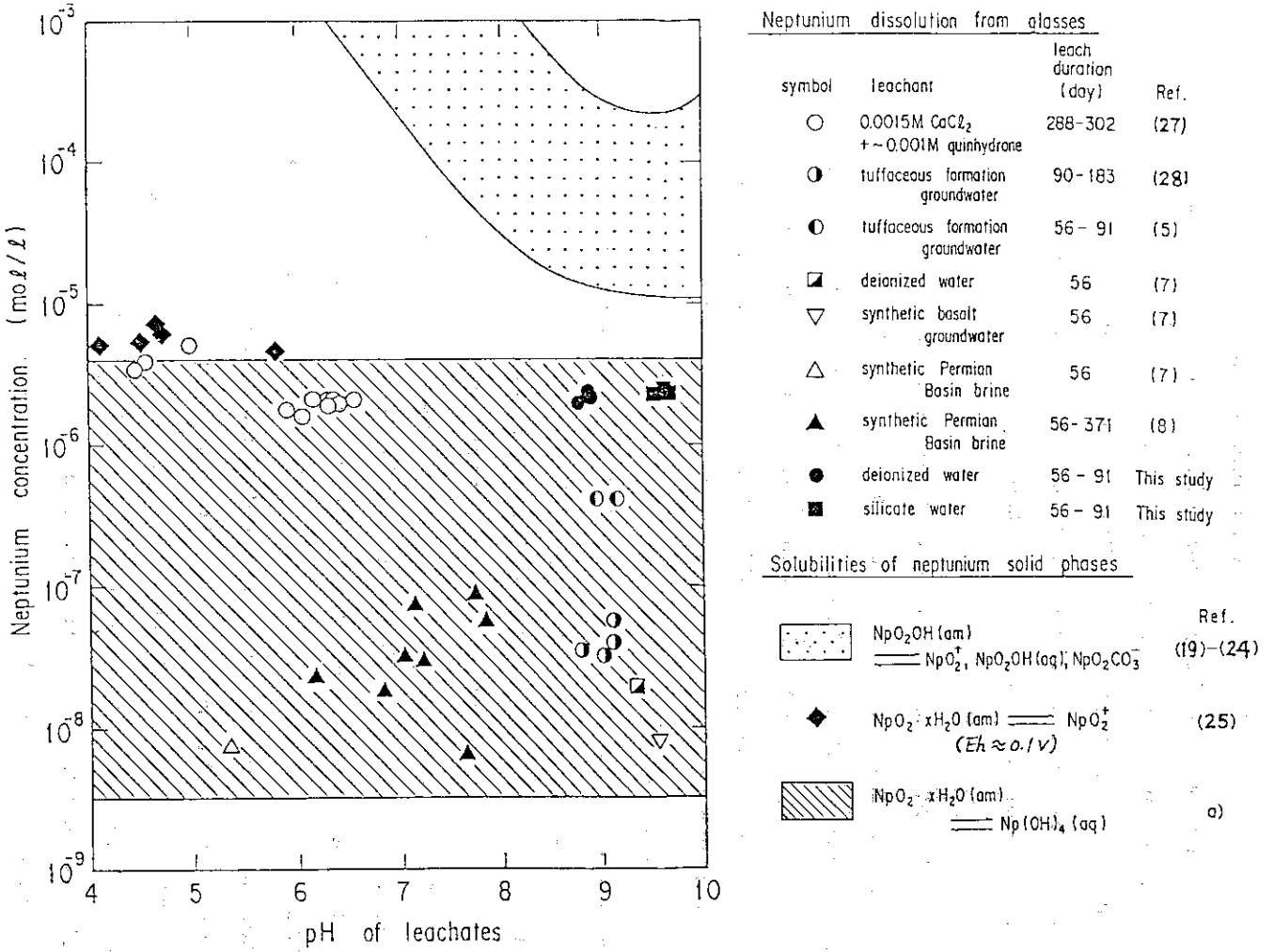

Fig. 4 Neptunium concentrations in glass leachates obtained from the MCC-1-type static leach tests for durations of 56 days or longer, and expected solubilities of $NpO_2 \cdot xH_2O$(am) and NpO_2OH(am) based on thermodynamic data. a) The concentrations of $Np(OH)_4$(aq) were calculated based on available data on the solubility product K_{sp} ($\log K_{sp}$=-54.5 for ionic strength I(mol/l)=0.0,[18] =-53.3 for I=0.025-0.044,[18] and =-51.4 for I=0.3[25]) and the hydrolysis constant K (logK=46) for $Np^{4+}+4OH^- = Np(OH)_4$.[26]

1.3 Volatilization of radionuclides from actual high-level waste

(1) Volatilization of ^{137}Cs and ^{106}Ru from borosilicate glass containing actual high-level waste

H. Kamizono

In the present study, attention is focused on safety in relation to operation of a storage facility. The volatilization of some radionuclides from borosilicate glass containing actual HLW generated at the Tokai Reprocessing Plant of the Power Reactor and Nuclear Fuel Development Corporation was examined in an almost closed canister.

The HLW glass used for the present study was borosilicate glass. The reagents for the glass additives and the simulated HLW which should be converted into 1300g of oxide glass were mixed simultaneously and placed in a vitrification apparatus with about one liter of a denitrated actual HLW solution. About 50g of various oxides were assumed to come from the actual HLW solution. This mixture was calcined at about 750°C, melted at 1200°C for 2 h in the vitrification apparatus. Half the molten glass was poured into an 8.1-cm-i.d., 24.4-cm-high stainless steel canister, kept at 600°C for 2 h, and then cooled to room temperature at a cooling rate of less than 40°C/h.

The experimental details in relation to the furnace and the sampling of the air inside the canister were described in Ref.1. The following is a summary, and additional information. The furnace temperature was raised in steps from 25°C to 1000°C. The temperature rise by the decay heat of the HLW was so small in the present study that it did not affect the temperature control of the glass.

During the course of heating, part of the air in the upper space of the canister was collected in an evacuated sampling bottle with a volume of about 7 cm^3. An important factor is the position of the hole in the sampling needle. It should be placed in the side of the needle in order to prevent it from being blocked by silicon rubber when the needle is inserted into the sampling tube. Radioactivity from volatile elements trapped by both the sampling bottle and the sampling needle was measured by an intrinsic Ge solid state detector which has a better resolution than the NaI(Tl) detector used in the previous study [1].

Figure 1 shows the temperature-dependence of volatility of ^{137}Cs and ^{106}Ru at a fixed time of 24 hours when both nuclides are at

apparent saturation concentrations. The solid line in the figure represents the data obtained in our previous work [1] in which the activation energy of about 140 kJ/mol was obtained on simulated HLW glass containing about 1.6×10^{10} Bq of ^{134}Cs. The present data shows fairly good agreement with this.

The volatility of ^{106}Ru measured at 600°C and 800°C is about one fifth that of ^{137}Cs. Since Gray [2] has pointed out that the activation energy for various elements are almost the same as each other, the air contamination of ^{106}Ru at a usual storage temperature of 400°C is also expected to be one fifth that of ^{137}Cs; thus, the normalized concentration of ^{106}Ru would be about 5×10^{-10} (Bq/cm^3-air)/(Bq/cm^3-glass) at 400°C. This extrapolated value may be conservative, since 400°C is below the softening point of the present glass and diffusion may not be a significant mechanism at this temperature. It should be also mentioned that the volatility of ^{106}Ru at 1000°C could not be measured; it was under the detection limit of 5×10^{-2} Bq/cm^3. This is probably an example that the backward step plays an important role; the stainless steel canister is markedly oxidized at around 1000°C and reacted with ^{106}Ru in the air inside the canister.

References

1. H. Kamizono, S. Kikkawa, S. Tashiro and H. Nakamura, "Volatilization of Cesium from Nuclear Waste Glass in a Canister," Nucl. Technol., 72, 84-88 (1986).
2. W.J. Gray, "Volatility of Some Potential High-Level Radioactive Waste Forms," Radioact. Waste Manage., 1, 147-149 (1980).

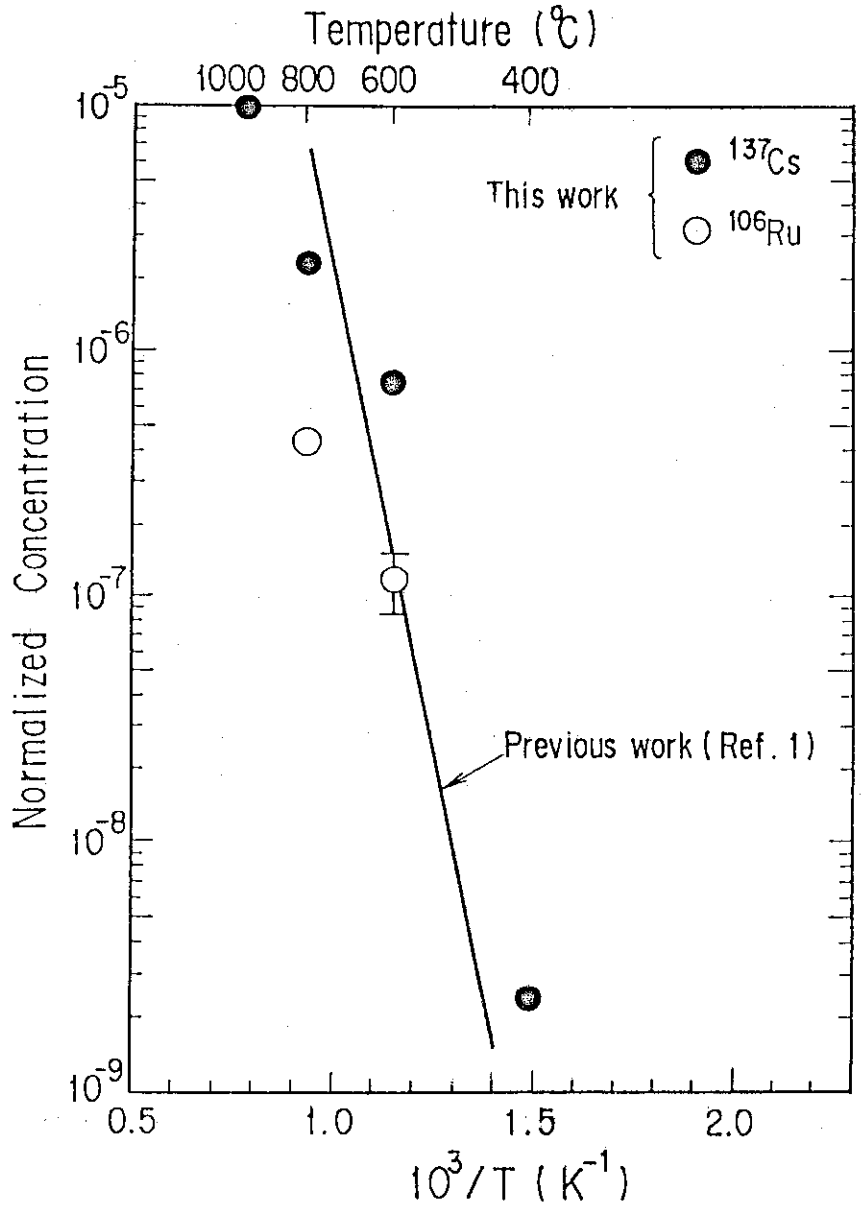

Fig. 1 Temperature-dependence of the volatility of ^{137}Cs and ^{106}Ru.

(2) Elemental analysis of the supernatant of actual high-level radioactive liquid waste

T. Banba

Under the cooperative research between PNC (Power Reactor and Nuclear Fuel Development Corporation) and JAERI (Japan Atomic Energy Research Institute), the studies on the safety evaluation of waste forms vitrifying the actual high-level radioactive liquid waste (HLLW) which was generated from the Tokai Reprocessing Plant, PNC, have been started. Prior to the tests, the 17 elements in the supernatant of actual HLLW were analyzed by means of the Inductively Coupled Plasma Atomic Emission Spectroscopy (ICP-AES) and the nonflame, Atomic Absorption Spectrometry (AAS). Although the ICP-AES was useful for almost all of elements, the nonflame AAS was more effective for the elements such as Na, Cs, Rh and Te than the ICP-AES. The results are shown in Table 1. All elements except Te and P were determined with the relative standard deviations in the 0.5 - 4.5 % range. And the results analyzing the simulated HLLW were within at least 10 % of the prepared concentrations for all elements except Zr and P. Both the reproducibility and accuracy are sufficient to indicate that the combination of the two analytical methods may be a viable technique for the determination of elements of actual HLLW. Since the poor reproducibilities of Te and P may be due to the poor sensitivity, the improvement in our current analytical technique would be required.

One of the most specific characteristics of the PNC waste was the large content of Na, i.e., 38.5 % as Na_2O. The low analyte concentrations of Zr, Mo and Ru in the supernatant of actual HLLW are probably attributed to the undissolved solids, e.g., zirconium molybdenum oxide hydroxide hydrate, $ZrMo_2O_7(OH)_2(H_2O)_2$[1], formed during storage.

Reference

1. Anderson, P.A. Laboratory simulation of high-level liquid waste evaporation and storage. Nucl. Technol. 47: 173 (1980).

Table 1 Analytical results of the supernatant of the actual PNC high-level radioactive liquid waste.

Element	Analyte concentration (g/l)	Rel. standard deviation (%)	Element	Analyte concentration (g/l)	Rel. standard deviation (%)
Sr	0.63	0.94	La	0.83	0.93
Zr	0.74	2.1	Ce	2.1	4.0
Mo	0.84	2.0	Nd	2.8	3.3
Ru	1.0	2.2			
Rh*	0.33	2.1	Na*	16	1.8
Pd	0.59	4.5	P	0.78	36
Te*	0.13	11	Fe	3.5	0.32
Cs*	1.7	1.7	Cr	0.44	1.9
Ba	1.3	0.56	Ni	0.79	2.6

*: These elements were analyzed with nonflame AAS.

1.4 Change in density of curium-doped Synroc due to self-irradiation

H. Mitamura, S. Matsumoto, Y. Togashi,
and S. Tashiro

Introduction

High-level nuclear waste (HLW) contains a lot of actinide elements which cause self-irradiation damage in ceramic waste forms. This damage can deleteriously affect stability of the waste forms, for example, by inducing dimensional changes that lead to cracking and a concomitant increase in surface area exposed to leachant. In our alpha radiation stability test, an acceleration method involving doping with a short-live actinide nuclide, ^{244}Cm, was used to assess the effect of self-irradiation damage on long-term stability of a ceramic waste form named Synroc [1].

Estimation of Synroc age

Synroc was assumed to contain 10 wt% of 5-year-old as-calculated HLW, or "JW" [2], from reprocessing of 2.41 % enriched UO_2 fuel which was burned up to 2.85 $TJ.kg^{-1}$ (33 $GWd.Mt\text{-}UO_2^{-1}$). In this waste, 56.57 kg of waste oxides was originated from reprocessing of the 1-Mt UO_2 fuel [2]. Under these initial conditions, each simultaneous equation on four decay chains for the actinide nuclides was solved with a computer by the Gear method [3] to obtain cumulative alpha decays in Synroc as a function of age (Fig. 1).

Experimental

Sample preparation

Synroc slurry mixed with curium solution was calcined at 750°C for 2 h and then hot-pressed at 1200°C and 29 MPa for 2 h in a hot cell [4]. Specific ^{244}Cm activity was 20.6 $GBq.g^{-1}$, as of November 1, 1987 [4]. Hereafter, this value will be adopted as the specific alpha activity in curium-doped Synroc since the total alpha activity of impurities was less than 0.4 % of that of ^{244}Cm.

Before density measurement, the peripheries of 2-cm-diam., 1-cm-high Synroc blocks were polished with #600 grit abrasive paper, and flat faces were finished with 6-μm diamond paste in the hot cell. Average density of the four block samples were 4.305 $g.cm^{-3}$ a month after hot pressing [4].

Density Measurement

Density measurement for one of the polished block samples, which was named as S87011, has been periodically carried out by water displacement method. After the sample was subjected to 15-minute ultrasonic washing with ethanol and then dried at 110°C for 1 h, its dry weight was measured with the electronic balance in Fig. 2. The hot-cell densimeter in this figure is automatically loaded and unloaded with the Synroc block using the sample changer. Water in the water vessel of 134 mm in diameter has been unperiodically replaced by fresh distilled water. Before the measurement, a water level in the water vessel was checked with the level sensor. When the water level gets low due to evaporation, distilled water is added to the water vessel until the water level reaches the level sensor. The level sensor therefore guarantees to keep the water level constant during the measurement. Nickel wire of 0.3 mm in diameter is adopted to make a wire net and hang the block sample on the wire net. Preliminary calculation has indicated that the fine nickel wire causes only negligible influences of surface tension of water and change in the water level on the density measurement when the sample is put into water. Water temperature in the water vessel is kept at 30(±0.5)°C with the sheathed ring heater in the water bath.

Results and discussion

Change in density is plotted in Fig. 3 with cumulative alpha decays as well as equivalent Synroc age. If the density, d, is assumed to decrease in accordance with the following equation [5]:

$$(d-d_o) = (d_s-d_o)(1-\exp(-kD)) \quad (1)$$

where d_o and d_s are the initial and the saturated densities, respectively, k is a constant related to damaged area per alpha decay, and D is cumulative alpha decays in unit of g^{-1}, then the least-squares method on the data gives the following figures as the fitted values: d_o and d_s are 4.3069(±0.0015) and 3.8413(±1.0482) $g \cdot cm^{-3}$, respectively, and k is 1.359(±3.234) $\times 10^{-19}$ $g \cdot \alpha^{-1}$. These parameters give a solid line in Fig. 3, which traverses all of the error bars attached to the data. Since standard deviation for initial density is sufficiently samll, the fitted value of d_o seems to have a high reliability. When the ratio of the fitted initial density to the least damaged density a month

after hot-pressing is supposed to be available for extrapolation to initial densities of the other block samples, their average density just after hot pressing must be 4.310 $g \cdot cm^{-3}$.

Equation (1) can be revised to an general form as follows:

$$\Delta d/d_o = A(1-\exp(-BD)) \qquad (2)$$

where Δd is an increment of density, A and B are constants, and the unit of D is converted to alpha decays$\cdot cm^{-3}$ here for convenience. The values of A and B for the present measurement are shown in Table 1 together with reference ones [5,6]. Table I implies that an increment of Synroc density might reach -11%, which is larger than the saturated increment of densities of the any other materials. A large change in density may occurs actually since another Synroc sample sustained an unsaturated volume swelling of 7.4 vol% by neutron irradiation equivalent to 0.7-million-year Synroc age [7].

References

[1] A. E. Ringwood and P. M. Kelly, "Immobilization of high-level waste in ceramic waste form," Phil. Trans. R. Soc. Lond. A. 319, pp.63-82 (1986).

[2] T. Banba, H. Kimura, H. Kamizono, and S. Tashiro, "Simulated HLLW Composition for cold test of waste management development," JAERI-M 82-088, Japan Atomic Energy Research Institute, Tokai (1982).

[3] G. D. Byrne, A. C. Hindmarsh, K. R. Jackson, and H. G. Brown, "A comparison of two codes: GEAR and EPISODE," Computer and Chem. Engineering, 1, pp.133-147 (1977).

[4] H. Mitamura, S. Matsumoto, W. J. Buykx, and S. Tashiro, "Fabrication of curium-doped SYROC for an alpha radiation stability test," Nucl. Technol., 85, pp.109-117 (1989).

[5] R. P. Turcotte, J. W. Wald, F. P. Roberts, J. M. Rusin, and W. Lutze, "Radiation Damage in Nuclear Waste Ceramics," J. Amer. Ceram. Soc., 65[12], pp.589-593 (1982).

[6] W. J. Weber and H. J. Matzke, "Radiation effects in actinide host phases," Radiation Effects, 98, pp.93-99 (1986).

[7] J. L. Woolfrey, K. D. Reeve, and D. J. Cassidy, "Accelerated irradiation testing of Synroc and its constituent minerals using fast neutrons," J. Nucl. Mater., 108 & 109, pp.739-747 (1982).

Table 1 Comparison of constants in the exponential fitting equation[a] for density change owing to ^{244}Cm doped.

Sample	A x10^2 (%)	B x10^{18} (cm^3)	A.B x10^{20} (cm^3)	Content of ^{244}Cm (wt%)
Synroc[b]	-10.8(±24.3)	0.032(±0.075)	-0.34	0.69
$CaZrTi_2O_7$[c]	-5.7	0.11	-0.60	3
$Gd_2Ti_2O_7$[c]	-4.9	0.12	-0.56	3
$Ca_2Nd_8(SiO_4)_6O_2$[c]	-7.4	0.22	-1.6	1.2
Supercalcine[d]	-1.47	0.6	-0.88	2
Glass Ceramic[d]	-0.470	1.5	-0.71	0.9
Glass[d]	-0.175	1.7	-0.30	0.9

(a) $\Delta d/d_0 = A(1-\exp(-BD))$ where A and B are constans, D is cumulative alpha decays in unit of $\alpha.cm^{-3}$.

(b) This work. Standard deviation for each constant is shown in parenthesis. The value of B is revised using the fitted initial density.

(c) After Weber and Matzke (1986). In this reference, volume swelling has been fitted by the equation of $a(1-\exp(-bD))$, where a and b are constants, D is cumulative alpha decays in unit of $\alpha.cm^{-3}$. The constants A and B in the present table are corrected by the equations of $A=-a/(1+a)$ and $B=(1+a)b$, respectively, and therefore $AB=ab$.

(d) After Turcotte et al. (1982).

JAERI-M 89-192

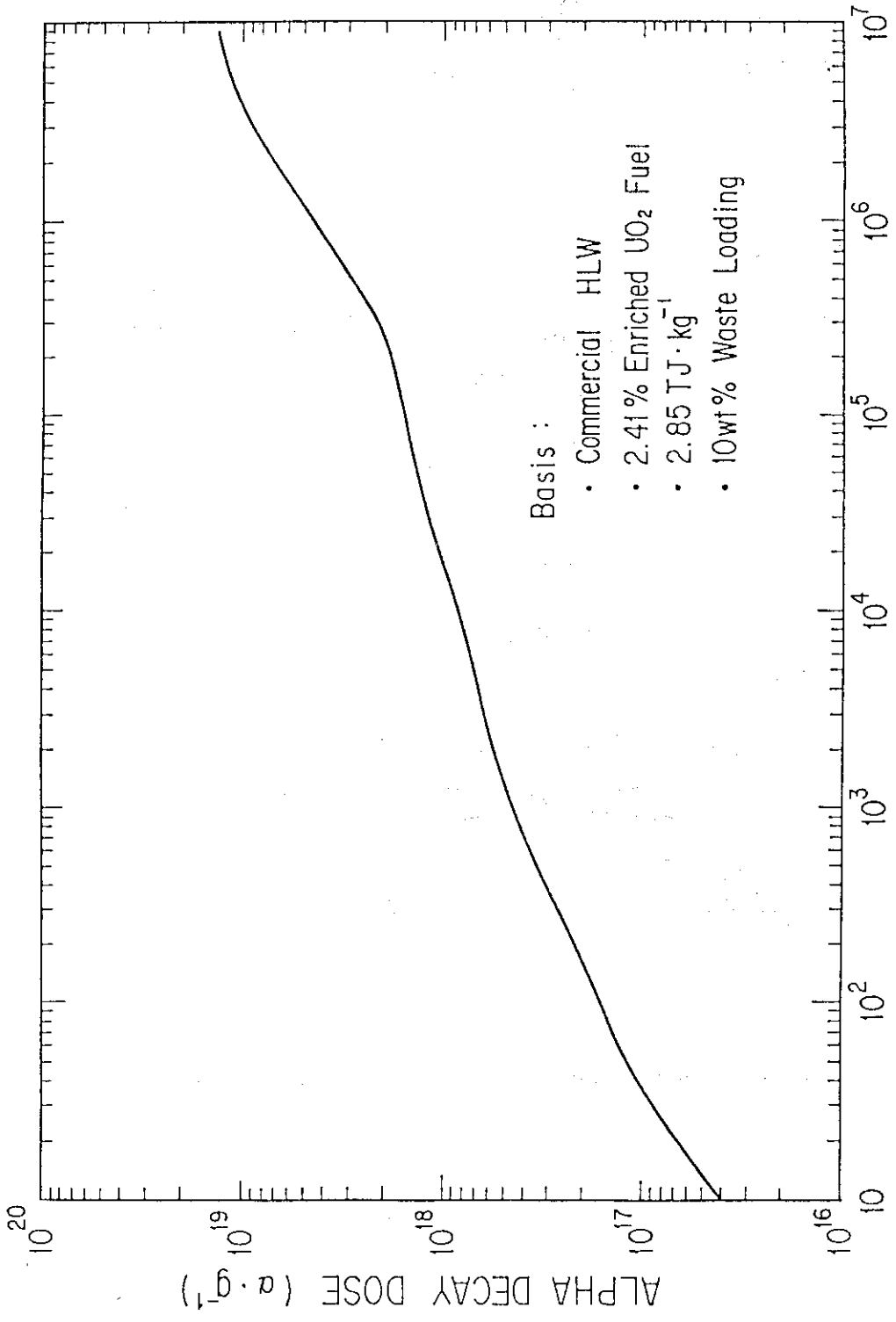

Fig. 1 Calculated cumulative alpha decays in Synroc against age. Synroc is assumed to contain 10 wt% of commercial HLW which is originated from spent uranium-dioxide fuel burned to 2.85 $TJ.kg^{-1}$ (Ref.2).

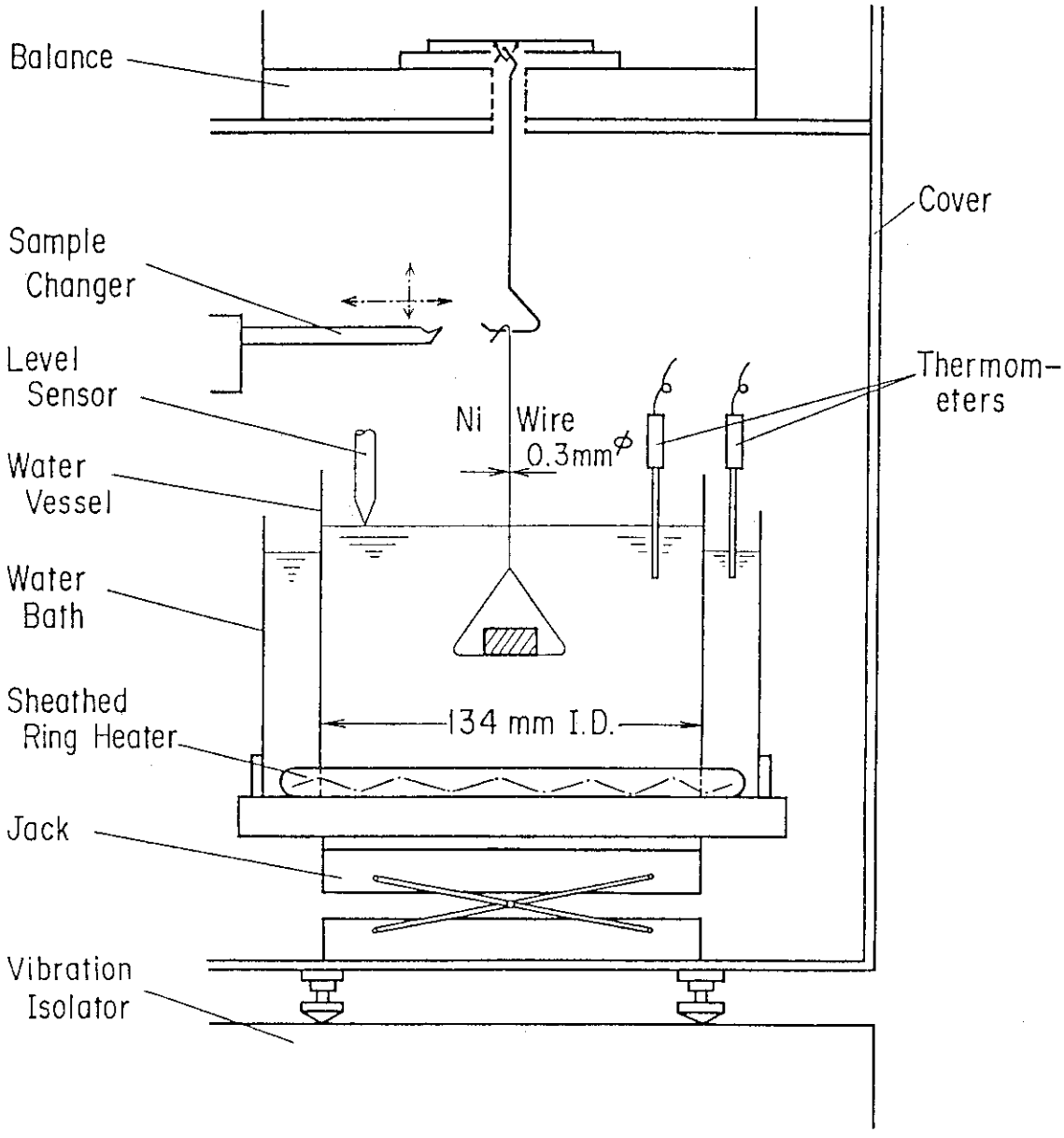

Fig. 2 View of in-cell apparatus for density measurement.

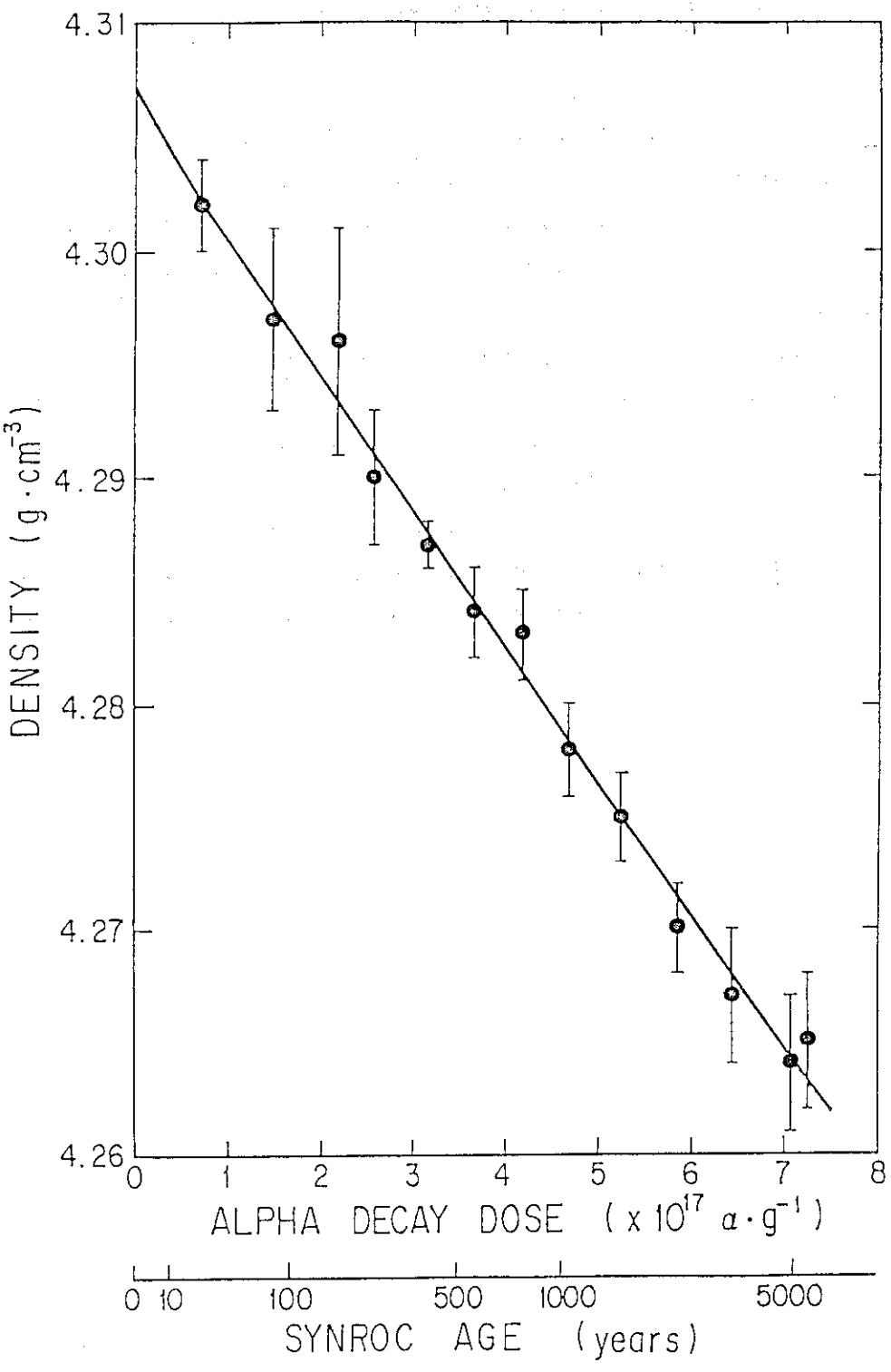

Fig. 3 Density change in curium-doped Synroc against cumulative alpha decays. Equivalent age of Synroc containing 10 wt% of commercial HLW is also shown. Solid line is derived from fitting by use of Eq.(1).

2. Safety evaluation for geological disposal

H. Nakamura

Migration through single fracture by slow convection and diffusion in non-fractured rock were studied using I^- and Sr^{2+} non-radioactive tracers, which are considered as the important processes controlling the time for leackage of radioactive nuclides to biosphere. The most emphasized researches were to estimate the long-term chemical behaviors of transuranium elements in geosphere. The one is laboratory experiment of adsorption of neptunium on natural occurring iron-containing minerals. The other is geochemical research on long-term reaction path modeling of radionuclide fixation.

In order to pick up the important items for the safety researches scenarios and data bases for the assessment were listed as the first version which will be revised a few times to be more reasonable and updated.

2.1 Studies on migration of redionuclides

(1) An experimental study on nuclide migration in simulated single fractures in granite

K. Nishiyama

Introduction

In safety evaluation of geological disposal of high level radioactive waste, it is important to study radionuclide migration in fractured rocks. In order to obtain fundamental data on radionuclide sorption capacity and retardation mechanisms in fractured rocks, nuclide migration experiments have been carried out with granite columns having simulated single fractures of 0.1~0.2 mm width. The main interest is to study the dependence of the diffusion coefficient and the retardation factor in the fracture on the water velocity. In this paper the first results on the permeability of the columns are described.

Experimental

The experimental apparatus is shown in Fig. 1. It consists of a tracer tank, a water tank, and two overflow tanks. The overflow tanks give pressures to six columns simultaneously. The columns are acrylic sylinders in which fractured granite blocks are fixed by epoxy resins to avoid the leak of water. The granite was taked from Inada, Ibaraki, Japan. As shown in Fig. 1 (b). The fractures were simulated by putting two granite blocks ($20\times40\times400^{1}$ mm) togerther with inserting teflon films as spacers of desired thickness. The water was injected into the fractures from the bottom of the column until constant velocity was obtained. The tracer solution was then injected. The tracer solution contained iodide (I^-, 130 ppm) and strontium (Sr^{2+}, 1.4 ppm). These ions are representatives of a non-sorbing and a sorbing tracers, respectively. Their concentrations in solutions eluted from the column were determined by Inductively Coupled Plasma-Atomic Emission Spectroscopy for Sr^{2+}, and Ion chromatography for I^-.

Results

The permeability coefficients for the fractures were calculated to examine the correlation between hydraulic gradients and flow rates through the column (Fig. 2). The results are shown in Table 1.

Fracture width was calculated by using the following equation (1) on a flow of viscous fluid in parallel interstice[1]. Eq.(1) is expressed by

$$k = \frac{1}{12} \frac{g}{\nu} w^2 \qquad (1)$$

in which k: permeability in single fracture, g: acceleration of gravity, ν: kinematic viscosity of fluid, w: width of fracture. Thier results in Table 1 agreed with surface fracture width measured by a peak stand microscope.

At present, the migration experiments using Sr^{2+} and I^- have been carried out for only two cases. The breakthrough curve is shown in Fig. 3. Future several experiments with various velocities in single fracture are being conducted in order to study the nuclide migration behavior in fractured rocks.

Reference

1. SNOW.D.T. (1968): Rock fracture spacings, openings and porosities, J. Soil Mech. Fonud. Div. Proc. ASCE, Vol.14, NO.SM1.

Table 1 Fracture width and permeability.

column No.	length (cm)	fracture width w (mm)		calculated c) permeability k (cm/s)
		surface a)	calculated b)	
1	37.9	0.15	0.14	1.61
2	38.0	0.14	0.15	1.82
3	37.1	0.15	0.18	2.75
4	36.9	0.12	0.11	0.91
5	35.8	0.09	0.10	0.81
6	33.5	0.12	0.09	0.70
7	36.3	0.22	0.22	3.89
8	30.2	0.20	0.21	3.52
9	29.0	0.21	0.22	4.02
10	36.3	0.13	0.13	1.28
11	35.0	0.15	0.10	0.88

a) measured by peak stand microscope.
b) calculated by using the following equation (1).
c) calculated by using the following equation (2).

Eq.(2) is expressed by

$$q = k A i \quad (2)$$

by Darcy's law

in which q: flow rate, A: flow section area, i: hydrauric gradient, k: permeability.

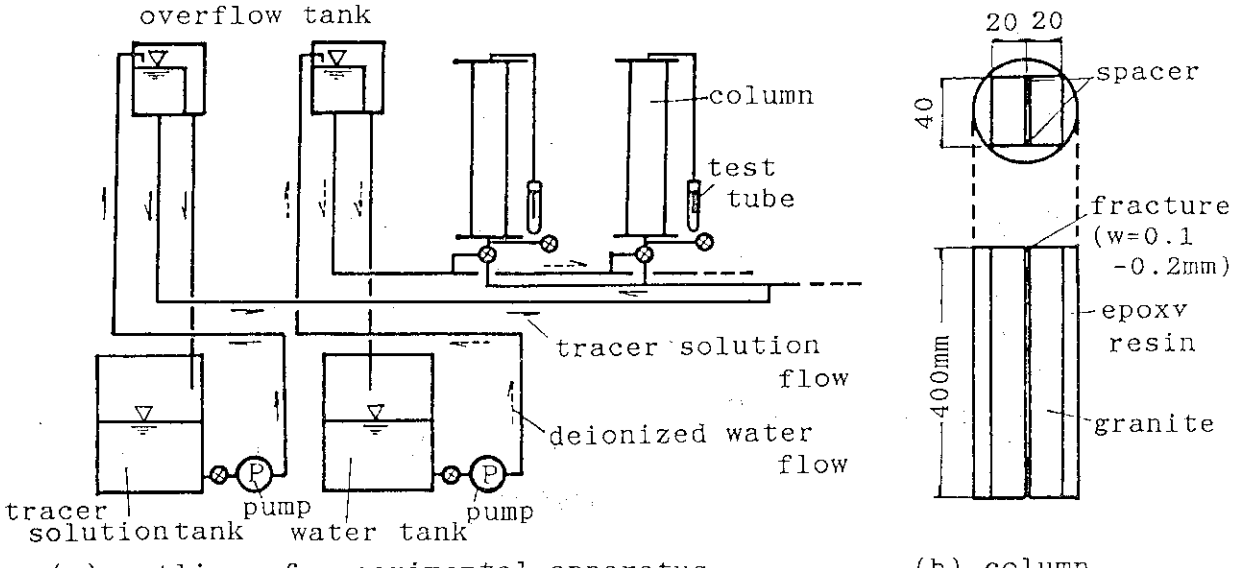

(a) outline of experimental apparatus (b) column

Fig. 1 Nuclide migration experimental apparatus.

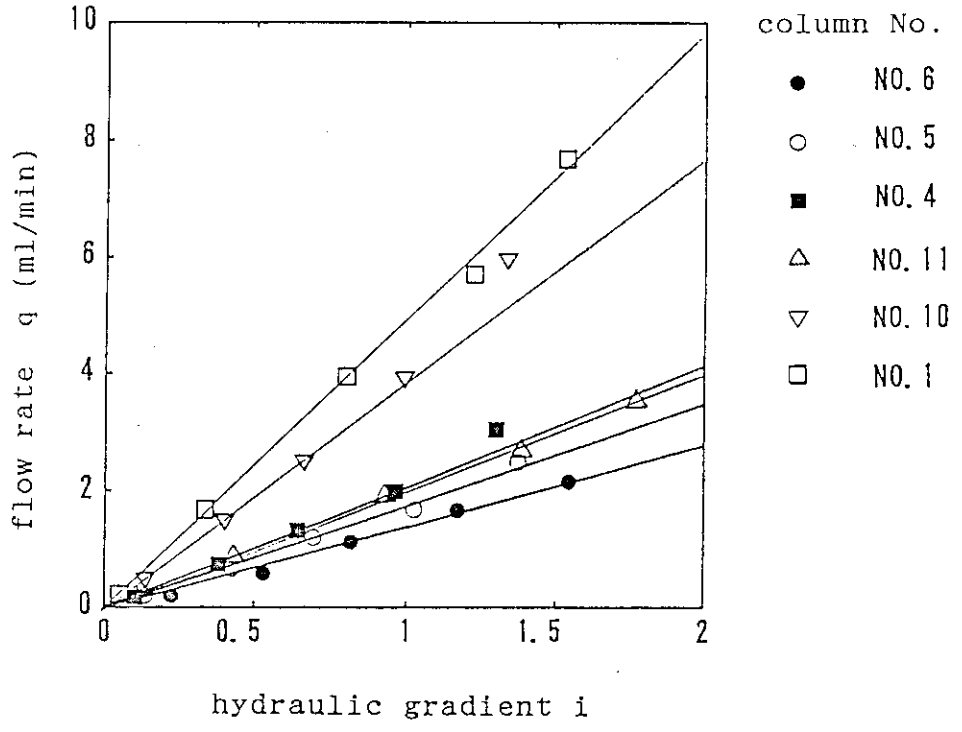

Fig. 2 Relation between hydraulic gradient and flow rate. (water temperature = 20°C)

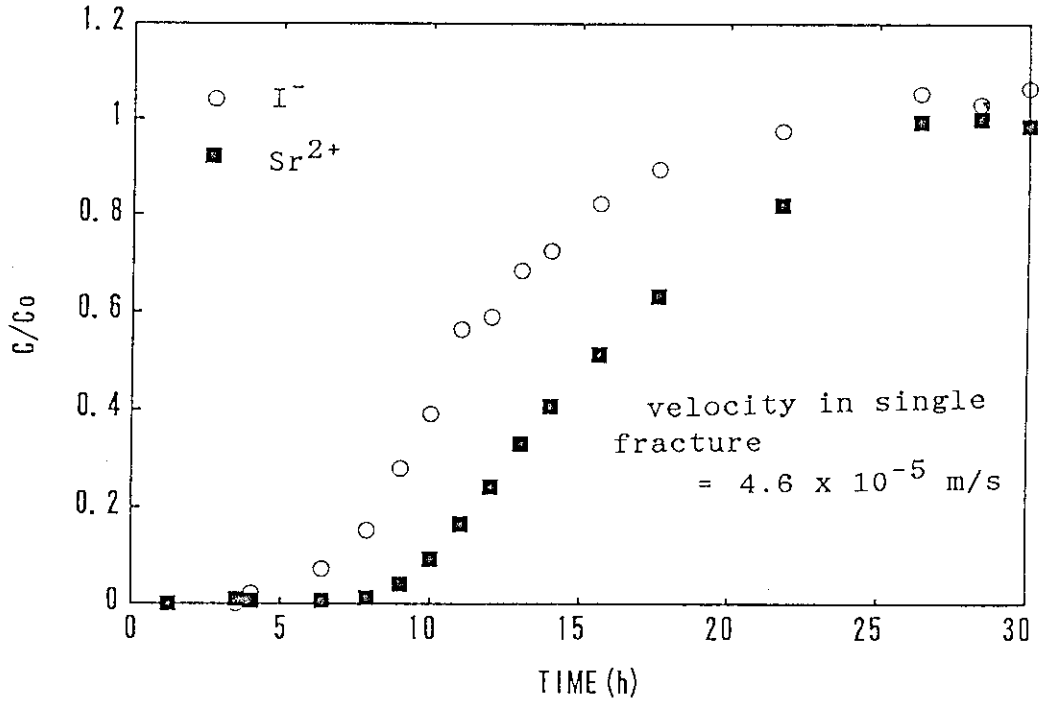

Fig. 3 Experimental breakthrough curve of column No.9.

(2) Porosities and diffusion coefficients of iodide anion in rocks

K. Nishiyama, S. Nakashima and T. Nagano

Introduction

The diffusion experiments of iodide anion have been carried out on granites and gneisses by SKAGIUS and NERETNIEKS[1]. They reported that diffusivities of iodide anion could be correlated roughly with porosities of rock matrix. However, it is doubtful whether the linear relation in a logarithmic diagram is applicable to various rocks, since their rock samples have very low porosities of 0.001~0.005. We have studied the diffusion of iodide anion on granites and tuffs[2]. Then, in this paper, we have carried out the diffusion experiments on andesites from Kushikino with porosities of about 0.15 and siliceous sedimentary rocks from Onnagawa with porosities of 0.04 and 0.13, in order to verify whethere there is a logarithm linear correlation between the effective diffusion coefficients and the effective porosities.

Experimental

The experiments were carried out on rock samples (ϕ=20mm, L=5mm), using 1M KI solution as a source of iodide anion (I^-). The method was in principle the same as that has been used previously by SKAGIUS[1] and KITA[2].

Results and discussion

The concentrations of iodide anion in an output diffusion cell, which has diffused through rock samples as a function time, is fitted to straight lines by the asymptotic solution of the diffusion equation. Effective diffusion coefficients D_e can be calculated from the gradient of the lines[1],[2].

The results on diffusion coefficients for andesites and siliceous sedimentary rocks were obtained to be $7.0\sim9.0 \times 10^{-12}$ m^2/s and $6.0 \times 10^{-12} \sim 1.2 \times 10^{-11}$ m^2/s, respectively. The data are plotted in Fig. 1 as the correlation between porosities and diffusivities. The straight line in Fig. 1 indicates a fitted line of SKAGIUS's data by a least-squares method. The data points for the andesites and the siliceous sedimentary rocks obtained in this study are located roughly on the extension of this fitted line.

Future diffusion experiments on various rock samples are being conducted in order to study in detail the correlation between porosities and diffusivities together with the dependence of diffusivity on the pore structure and the tortuosity of rock matrix.

References

1. SKAGIUS, K. and NERETNIKS, I. (1986): Porosities and diffusivities of some nonsorbing species in crystalline rocks, Water Resource Research, Vol.22, No.3, pp.389-398.
2. KITA, H., IWAI, T. and NAKASHIMA, S. (1987): Diffusion of ions in rock pore water, Collected papers presented at the Annual Meeting of the Japan Society of Engineering Geology, pp.45-48.

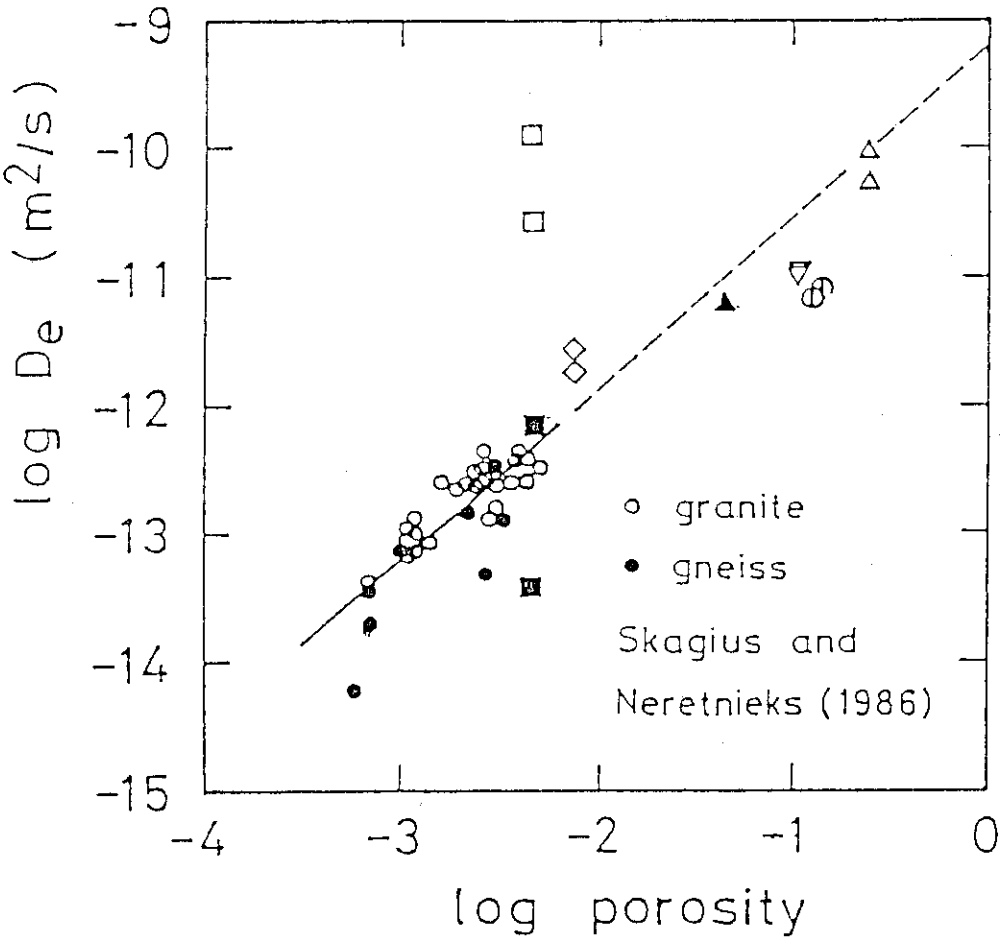

Fig. 1 Correlation between the effective diffusion coefficients of iodide anion and the effective porosities of various kind of rocks.
○,●: granite and gneiss from Sweden (Skagius and Neretnieks 1986)
◇ : granite from Inada; ⌀: andesite from Kushikino
△ : tuff from Izu; ▲,▽: siliceous sedimentary rocks from Onnagawa
□,■: schists from Iwaki whose schistosity are parallel and perpendicular to the diffusion direction.

(3) Adsorption of neptunium on naturally occurring iron-containing minerals in aqueous solutions

S. Nakayama and Y. Sakamoto

Introduction

Neptunium is an important radionuclide in safety assessment of geologic disposal. The sorption properties must be primarily studied to predict the behavior in the geosphere.

In aqueous solutions neptunium is a redox-sensitive element. Under oxidizing conditions, neptunium exists as NpO_2^+, in the pentavalent state, and shows little sorption by geologic materials. Under reducing conditions, or in the absence of oxygen, neptunium exists as tetravalent state. The adsorption properties under reducing conditions have not been well known.

Iron is one of major components of minerals. In addition, much amount of iron will have been released from the corroded canisters into groundwater over a long timescale, and finally precipitate to form iron-containing minerals. Under reducing conditions like those in deep undergrounds, iron may exist as ferrous as well as ferric. Ferrous ion is known to reduce neptunium(V) to neptunium(IV) in solution. This leads to the increase in removal from solution either due to the low solubility limit or due to the enhanced sorption ability or both. For this reason, the mechanism of removal of neptunium from solution in the presence of iron-containing minerals is primarily to be studied.

In this report we describe the first result on neptunium adsorption on iron-containing minerals (hematite, magnetite, biotite, goethite) under oxidative (aerated) conditions.

Experimental

Hematite was obtained from Egremont, UK, magnetite from Kouchi, Japan, goethite from Mongolia, China and biotite from Nellore, India. These minerals were mechanically crushed to less than 100 μm in size, and washed by deionized water a few times before use. Usually 20 mg of the mineral was placed with 20 ml of a 0.1 M $NaNO_3$ solution in a polyethylene bottle and neptunium dissolved in a 0.1 M HNO_3 was added. The pH was adjusted by NaOH or HNO_3 to the value between 4 and 11. The bottles were shaked in a water bath at 30°C. After the desired

sorption duration the solid was separated from the solution by filtration (0.45 μm). The neptunium concentration in the solution was determined by using a liquid scintillation counter to calculate the adsorbed amount of neptunium.

Results and Discussion

Adsorption equilibria were attained within four hours for hematite, magnetite and biotite, and two days for goethite. Adsorption was reversible for the change in pH for all the minerals.

The dependence of adsorption behaviors of neptunium on pH is shown in Fig. 1. The dependence is different between goethite and other minerals remarkably; the adsorption on goethite represented a rapid increase at pH of 6 to 8 while that on other three kinds of minerals showed in pH above 9. This difference may be due to the difference in the mineral structures, i.e., the presence of OH in goethite(α-FeOOH) may contribute to the neptunium adsorption. In order to understand the mechanisms, further experiments have been conducted on other metal oxyhydroxides with similar molecular structures such as α-AlOOH and γ-FeOOH.

No evidence was observed in the short-term adsorption studied here that neptunium was removed from solution more by ferrous-iron-containing minerals than ferric-iron-containing minerals. The sorption experiments under unoxidative conditions are also in progress.

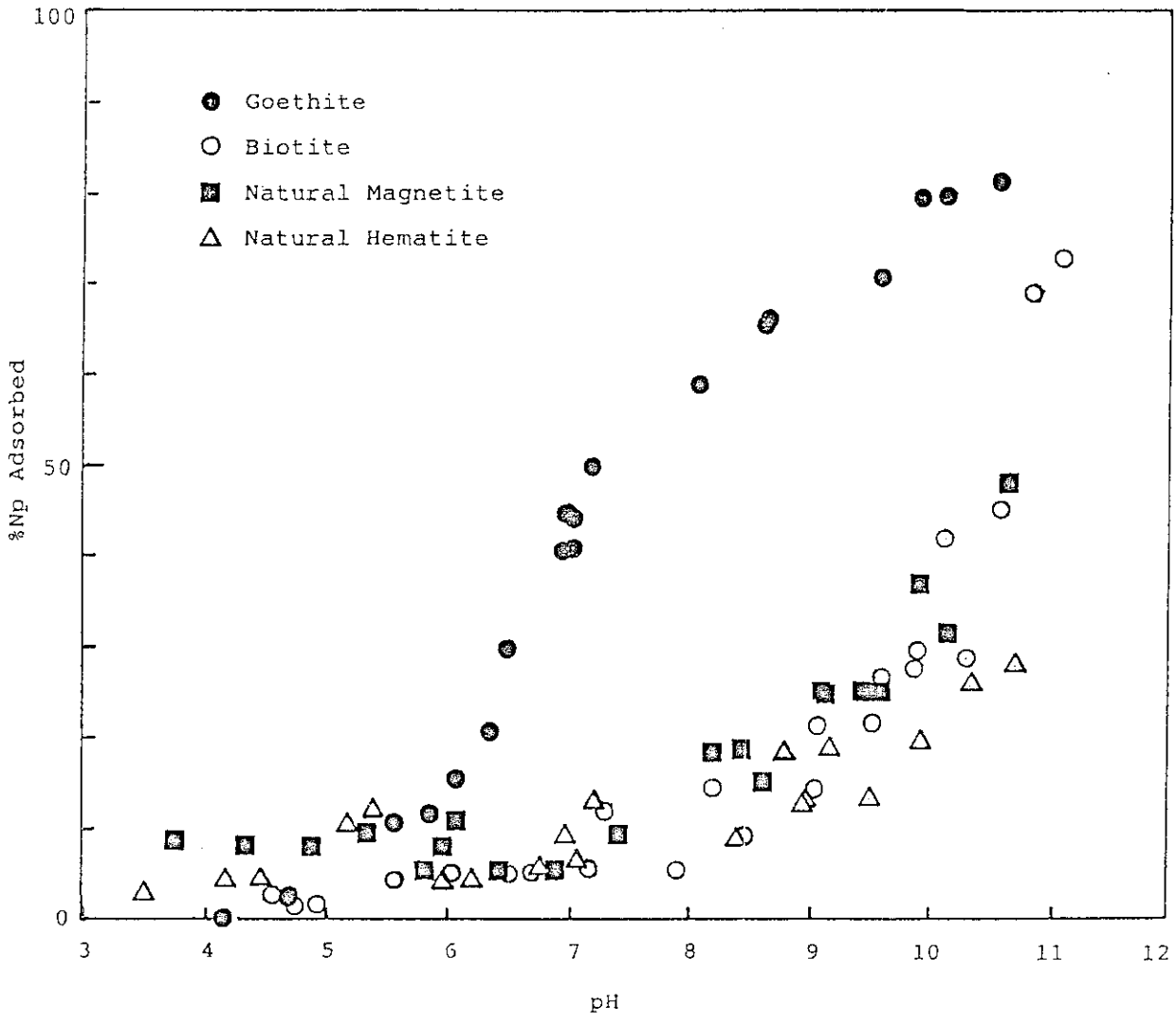

Fig. 1 Adsorption of neptunium on naturally occurring iron-containing minerals as a function of pH.

2.2 Long-term reaction path modelling of radionuclide fixation in geosphere by spectroscopic methods

S. Nakashima and T. Nagano

Abstract

As a first step of the reaction path modeling of the long-term behavior of iron during water-rock interactions, visible diffuse reflectance spectroscopy and infrared microspectroscopy have been applied to elucidate chemical forms of iron and water in granitic rocks. These spectroscopic methods revealed that at least a part of dissolved iron in groundwater is finally fixed in granitic rocks as ferric iron hydroxides and oxides. The site of its fixation is different due to the different geochemical environments: as ferric iron hydroxides around biotite during the weathering and as goethite and hematite inside feldspars near the fracture during the hydrothermal alteration. Different behavior of certain radionuclides such as Am, which is easily coprecipitated with ferric iron hydroxides and sorbed by some ferric iron minerals, is hence supposed in different geological environments.

Introduction

Application of natural phenomena to the safety evaluation of radioactive waste disposal has some advantages concerning the evaluation of long-term behavior of waste radionuclides, because this is difficult to be done only by laboratory experiments (Nakashima and Nakamura, 1987). The long-term behavior of waste radionuclides in geological formations can be simulated by that of certain natural elements during natural processes such as alteration and weathering of rocks. For considering quantitative aspects of the long-term behavior of natural elements, kinetic consideration is needed and in that case, reaction paths should be first modeled.

It is reasonable to consider that some trace radionuclides have similar behavior to certain natural elements. For instance, americium (Am) is reported to have a similar behavior to that of iron in natural environments (Vangenechten et al., 1987). In fact, in laboratory experiments, coprecipitation of Am with ferric hydroxides is well known. Am is also reported to form pseudo-colloids in aqeous solution with ferric hydroxides as the host colloid (Nakayama et al., 1986).

These amorphous iron hydroxides are considered to "evolve" with time in laboratory experiments toward crystalline phases such as goethite [FeO(OH)] and hematite [Fe_2O_3] (Van der Woude et al., 1983). Am is also easily sorbed by iron hydroxides and oxides during the batch sorption experiments (Goncharova et al., 1974). On the other hand, these iron hydroxides and oxides are the common products of water-rock interactions (Schwertmann, 1985). However, reaction paths of their formation in geological environments are not well known. The reaction path modeling of iron behavior during water-rock interactions is hence necessary for estimating the long-term behavior of certain radionuclides such as Am.

Some of typical examples of iron behavior during water-rock interactions are (a) brown staining of granitic rocks during the weathering process (alteration of rocks at the earth's surface) and (b) red coloration of granitic rocks along fractures. These phenomena are very common for granitic rocks, but it is not easy to determine the origins of color changes of rocks. This difficulty arises from the small amount of iron-bearing materials which exhibit reddish or brownish colors. Conventional analytical techniques such as electron probe micro-analysis and X-ray diffractometry are not able to detect and determine chemical states of iron-bearing phases. New analytical techniques are then necessary for the determination of chemical forms of these trace microphases.

Spectroscopic methods are considered to be most suitable for the study of origins of colors and chemical states of elements in rocks (Fawthorne, 1988). In order to elucidate chemical forms of iron in powdered rock samples, visible diffuse reflectance spectroscopy has been applied, and based on the spectroscopic results, the behavior of iron during the weathering of a granitic rock has been modeled.

Another important aspect of the reaction path modeling during water-rock interactions is the analysis of chemical states of water in rocks, because water is usually involved in the reaction mechanisms. Infrared spectroscopy has been used to analyze different states of water in rock-forming materials, especially in alteration products of rocks such as amorphous materials and clay minerals (Van Der Marel and Beutelspacher, 1976). We have developped a new technique of Fourier transform infrared microspectroscopy in order to study chemical states of water and its spatial distribution in microscopic areas of minerals

(Nakashima, 1987).

This paper describes the application of these spectroscopic methods to the study of reaction paths concerning the behavior of iron during the weathering and alteration of granitic rocks.

Experimental Methods

Visible Diffuse Reflectance Spectroscopy of Rock Powder

The color of a bulk rock can be analyzed by measuring the scattered visible light on the finely powdered rock sample (diffuse reflectance). This diffuse reflectance in the visible region provides data similar to visible absorption spectra on minerals, and so that gives information on valence states and coordination environments of transition metals in minerals (Adams, 1975).

60 mmϕ integrating sphere, of which inner part is covered with white material ($BaSO_4$), is installed in an ultraviolet-visible spectrophotometer Hitachi U-3210 to condense the diffuse reflectance light. A rock sample is ground in an agate and mounted in a sample container with a quartz window. Powdered white Al_2O_3 is mounted in a container as a reference material. The obtained diffuse reflectance in the wavelength range of 380 to 780 nm is represented quantitatively by the Kubelka-Munk function F(R). Using this quantity, one may relate diffuse reflectance spectra to absorption spectra (Sherman et al., 1982).

Fourier Transform Infrared Microspectroscopy of Rock Thin Section

Preliminary description of Fourier transform infrared (IR) microspectroscopy has been given in Nakashima (1987) and detailed description will be published later. The outline of the method is only summarized here.

An IR microscope JEOL IR-MAU110 was installed in a Fourier transform infrared spectrometer JEOL JIR-3505. Among three measurement methods tested (reflection, transmission-reflection, transmission; Nakashima, 1987), transmission measurement is found to be most appropriate for the analysis of water in minerals. A conventional rock thin section (about 30 μm thick) is polished up to micrometer diamond paste levels, and the glass plate and adhesive are finally removed off by organic solvent. The rock thin section is placed on a hole of a metal plate leaving a part of the hole open, and this metal plate is

placed on the sample stage of the IR microscope. A reference spectrum is first measured on the hole without the sample with a desired aperture, and then the same procedure is applied to the sample located in the hole to measure a sample spectrum. The ratio of these two spectra gives an IR transmission spectrum of the desired position of the sample. Final quantitative spectra are presented in an absorbance vs. wavenumber diagram.

Detailed mapping of 10 μm step on hydrous mineral inclusions in altered feldspars has been carried out in order to verify the spatial resolution of IR microspectroscopy for water in minerals. The results suggest that IR micro-mapping by IR microspectroscopy can provide information on spatial distribution of different states of water in minerals in areas as small as 10 × 10 μm.

Results and Discussion

(i) Behavior of iron during the weathering of a granitic rock

Weathering is a phenomenon that rocks are altered by surface water for a long period. In this study, weathered granitic rocks were analyzed with special emphasis on the behavior of iron during the weathering. Granitic rock samples were collected from a cliff near Mizunuma Dam, Kita-ibaraki, Ibaraki, Japan. This cliff can be classified into three major weathering zones A, B and C (Kunori et al., 1971). The weathering degree increases in the order of A, B and C.

X-ray diffractometry (XRD) on powdered rock samples reveals that the rocks are composed of four major mineral phases, namely quartz, biotite, K-feldspar and plagioclase, and that the peak height of biotite decreases as the weathering degree increases. Quantitative XRD analysis using an internal standard method enables the determination of biotite content in powdered bulk rocks. The result is shown in Fig. 1. The biotite content clearly decreases as the weathering degree increases, and this fact can be understood by the increasing dissolution of biotite in a geological time scale. The decrease of biotite content in bulk rocks can be taken as an indicator of the weathering degree.

Rock samples from the highly weathered zone (C zone) appears more brownish than those from less weathered zone (A zone) with the naked eye. Microscopic observation of the samples from the three different weathering zones shows that brown parts around biotites are origins of

the brownish color of the rocks. Moreover, an analysis by scanning electron microscopy equipped with energy dispersive X-ray analyzer (SEM-EDX) shows that these brown parts contain only Fe among elements heavier than Na. These are then suspected to be iron oxides or hydroxides.

The color of rock powders from each weathering zone was studied by means of visible diffuse reflectance spectroscopy. The typical result is shown in Fig. 2. A weak broad band around 480 nm appears to increase its absorbance as the weathering degree increases. As stated above, this band can be considered to be due to iron-bearing oxides, hydroxides or amorphous materials. As typical iron-bearing minerals, hematite [Fe_2O_3] and goethite [FeO(OH)] were subjected to diffuse reflectance spectroscopy. Fig. 3 indicates an interesting result that although both hematite and goethite contain Fe^{3+}, the spectra of the two minerais show different patterns, especially in the 380-600 nm region. This result means that discrimination between hematite and goethite can be made by means of diffuse reflectance spectroscopy. In fact, hematite appears reddish and goethite appears brownish with the naked eye. By comparison, the spectra of weathered granitic rocks (Fig. 2) are very similar to that of goethite (Fig. 3). Though spectra of amorphous FeO(OH) has not yet verified, the brownish color of the weathered granitic rocks is considered to be due to the presence of goethite-like ferric iron hydroxides. By assuming that these brownish materials can be treated as FeO(OH) for their chemical formula, the peak area around 480 nm is used to calibrate and calculate the FeO(OH) content of the granitic rocks. The FeO(OH) content of 18 rock samples are thus calculated as shown in Fig. 4. The increase of the FeO(OH) content due to the weathering is now obvious.

Based on the above results, the following hypothesis can explain the behavior of iron during the granite weathering: iron in biotite, mostly as Fe^{2+}, was dissolved into surface water and then precipitated as ferric iron-bearing minerals (tentatively as FeO(OH)) around biotite.

Laboratory experiments at around 25°C on the dissolution and precipitation of minerals suggest the very slow dissolution rate of biotite, probably in the order of 4×10^{-13} mol·m^{-2}·s^{-1} (Lin and Clemency, 1981) and the very fast precipitation of ferric iron hydroxides, probably in the order of 10^{-5} s^{-1} (Van der Woude et al.,

1983). The rate-determining step of the iron behavior during the granite weathering is therefore supposed to be the dissolution of iron from biotite. A preliminary calculation with some assumptions after the method described in Lasage (1984) on the dissolution rate of biotite for the weathered granitic rocks suggests the time required for the decrease of biotite from the weathering zone A to the weathering zone C (Fig. 1) to be in the order of 800 thousands of years. Though these quantitative parameters need to be verified by further experimental and theoretical studies, this consideration provides an approach for the quantitative evaluation of the long-term behavior of iron, which can be regarded as an indicator of behavior of certain radionuclides such as Am during low temperature water-rock interactions.

(ii) Behavior of Iron during the Hydrothermal Water-Rock Interactions

Another application of spectroscopic methods to the long-term reaction path modeling of trace elements during water-rock interactions has been made on the red coloration of granitic rocks along fractures. A granitic rock sample (Fig. 5) was collected from the central region of Saga Prefecture, Kyushu, Japan. This sample is altered by the penetration of hydrothermal solutions along a paleo-fracture which are now filled mainly with prehnite [$Ca_2(Al, Fe^{3+})_2Si_3O_{10}(OH)_2$]. Albite and chlorite are the main alteration products.

Red coloration of feldspars is observed about 1 cm in thickness along the paleo-fracture. Visible diffuse reflectance spectra on the powdered red feldspars (Fig. 6a) indicate that the reddish color can be attributed to the presence of both goethite [FeO(OH)] and hematite [Fe_2O_3] (Fig. 3 and Fig. 6b). In fact, the transmission electron microscopy reveals the dissemination of at least two different submicron iron minerals in the red feldspar. A quantitative spectral fitting of the red feldspar (Fig. 6a) by the composite spectra of goethite and hematite (Fig. 6b) suggests that the red feldspar may contain 0.17 wt% of goethite and 0.03 wt% of hematite.

These results permit a hypothesis on the iron behavior to be made: ferric iron in the hydrothermal solution has penetrated into the fracture of the granitic rock and diffused into the granite matrix through pore water, then precipitated as ferric iron microphases in feldspars having abundant micropores (Suzuki et al., 1989). The

presence of both hydrous and unhydrous ferric iron minerals suggests different degrees of hydration during the water-rock interaction.

It should be noted that the red coloration of granite exist mainly inside feldspars. It is then necessary to consider iron penetration mechanisms into feldspars. As stated above, this can be explained at least partly by the diffusion of iron through micropores of feldspars. If we suppose the effective porosity of feldspars to be in the order of 2 % (Suzuki et al., 1989), the diffusion coefficient of dissolved species through micropores can be in the order of 10^{-12} $m^2 \cdot s^{-1}$ (data at 25°C; Kita et al., 1989). Another possibility for the iron penetration into feldspars is the diffusion through hydrated surface layers of feldspars, which is supposed to be fast if these layers are composed of hydrous clays (typical diffusion coefficients in hydrous clays are about 10^{-10} $m^2 \cdot s^{-1}$ at 25°C; Berner, 1981).

The presence of chemically altered surface layers has long been assumed for leached minerals in the course of water-rock interactions, and the diffusion of elements through these layers are often assumed to be a rate-determining step of the reactions. However, the presence of hydrated surface layers has not been verified by conventional analytical techniques such as electron microscopy and X-ray photoelectron spectroscopy (XPS) (Lasaga, 1984). Recently, a resonant nuclear reaction (RNR) has been employed to do hydrogen depth profiling for dissolving minerals and glasses. This technique reveals the presence of hydrated surface layer of 0.05 - 2 μm thick at around 70°C. (Smets and Lommen, 1983; Petit et al., 1987). However, RNR analysis only reveals the presence of hydrogen in the surface layer and cannot discriminate between hydrogen-containing species (H^+, H_3O^+, H_2O, OH^-).

As stated above, the characterization of hydrous microphases is possible by means of infrared microspectroscopy. This method was therefore applied to a thin section of the hydrothermally altered granitic rock (about 30 μm thick) in order to study the hydrated surface layers of feldspars.

IR transmission spectra were measured on the thin section of the granitic rock shown in Fig. 5. Typical spectra for hydrous species present in the altered rock are presented in Fig. 7. The results of a line-profile analysis crossing the paleo-fracture and the adjacent red feldspar are presented in Fig. 8. By comparison with the data in Fig. 7, the IR spectra of fracture-filling materials (Fig. 8) indicates that

they are mainly composed of prehnite with some chlorite. The IR spectra for the feldspar grain adjacent to the paleo-fracture show about two times higher peak heights at 3622 cm^{-1} at the mineral surface (about 200 μm from the surface) than inner parts of the mineral (Fig. 8). The symmetric stretching vibration of O-H bonds appears in this spectral region from 3200 to 3700 cm^{-1}. Therefore, the above results indicate the presence of a hydrated surface layer of the feldspar grain. Moreover, the peak at 3622 cm^{-1} is considered to be mainly due to clay minerals such as sericite [$K_2Al_6Si_6O_{20}(OH)_4$]. Consequently, the hydrated surface layer can be mainly composed of this kind of clay, and so that the diffusion through this layer can be a possible mechanism for the iron penetration into the feldspar grain.

Based on all these spectroscopic results, the red coloration of the granitic rock along the fracture can be explained by the following hypothesis: (a) groundwater penetration into the granitic rock along the fracture and the formation of hydrated surface layers on feldspars near the fracture; (b) diffusion of dissolved iron in groundwater through the hydrated layers and/or micropores of feldspars; (c) iron precipitation as iron hydroxides-oxides (goethite and hematite) in micropores.

These reaction paths for the iron behavior during hydrothermal alteration are different from those presented above during the weathering of the granitic rock. Different behavior of certain radionuclides such as Am is hence supposed for two different water-rock interactions.

Conclusions

The long-term behavior of certain waste radionuclides such as Am in geological environments can be simulated by that of iron during several natural processes such as weathering and alteration of rocks. In order to model reaction paths concerning the long-term behavior of iron, spectroscopic methods has been applied to elucidate chemical forms of iron and water during water-rock interactions. Visible diffuse reflectance spectroscopy on powdered granitic rocks revealed the increase of ferric iron hydroxides following the weathering. Considering the decrease of biotite determined by X-ray diffractometry, the following behavior of iron has been hypothesized: ferrous iron is dissolved into groundwater from biotite and ferric iron

hydroxides are rapidly precipitated around biotite.

Infrared microspectroscpy has been developed and applied to a hydrothermally altered granitic rock in order to study chemical states of water and its spatial distribution in minerals. A hydrated surface layer was detected by this method on a red feldspar adjacent to the paleo-fracture. Visible diffuse reflectance spectroscopy on red feldspars reveals the presence of both goethite and hematite. Based on these spectroscopic results together with our porosity and diffusion data on granite, the following hypothesis can explain the dissemination of submicron iron minerals in feldspars near the paleo-fracture: (a) groundwater penetration into the granitic rock along the fracture and the formation of hydrated surface layers on feldspars near the fracture; (b) diffusion of dissolved iron in groundwater through the hydrated layers and/or micropores of feldspars; (c) iron precipitation as iron hydroxides-oxides (goethite and hematite) in micropores of feldspars.

These reaction paths for the iron behavior during two different typical water-rock interactions indicate the reaction paths and the rate-determining steps can be different for the iron behavior under different geological conditions. It should be noted, however, that at least a part of dissolved iron in groundwater is finally fixed in granitic rocks as ferric iron hydroxides and oxides. The site of its fixation is different due to the different geochemical environments: as ferric iron hydroxides around biotite during the weathering and as goethite and hematite inside feldspars near the fracture during the hydrothermal alteration. Different behavior of certain radionuclides such as Am, which is easily coprecipitated with ferric iron hydroxides and sorbed by some ferric iron minerals, is hence supposed in different geological environments even if the host rock is the same. The behavior might also vary with time as these iron minerals evolve in a geological time scale. Further studies of long-term reaction path modeling by means of spectroscopic methods and kinetic considerations are needed for the quantitative evaluation of the behavior of waste radionuclides in geomedia. (This is submitted to the Proceeding of the 1989 International Joint Waste management Conference Oct. 23-25; Kyoto)

Acknowledgements

The authors wish to thank Drs. Hirano and Nakamura of Japan Atomic Energy Research Institute for their support of this work.

References

1. Adams, J.B., 1975, "Interpretation of Visible and Near-Infrared Diffuse Reflectance Spectra of Pyroxenes and Other Rock-Forming Minerals," Infrared and Raman Spectroscopy of Lunar and Terrestrial Minerals, Karr, C., Jr. ed., Academic Press, New York, pp.91-116.
2. Berner, R.A., 1981, "Kinetics of Weathering and Diagenesis," Kinetics of Geochemical Processes, A.C. Lasaga and R.J. Kirkpatrick, eds., Reviews in Mineralogy Vol.8, Mineralogical Society of America, pp.111-134.
3. Fawthorne, F.C. ed., 1988, "Spectroscopic Methods in Mineralogy and Geology," Reviews in Mineralogy, Vol.18, Mineralogical Society of America, 698p.
4. Goncharova, L.K., Myasoedov, B.F. and Novikov, A.I., 1974, "Sorption of Americium in Different Oxidation States by Iron and Zirconium Hydroxides," Radiokhimiya, Vol.16, pp.308-312.
5. Kita, H., Iwai, T. and Nakashima, S., 1989, "Diffusion Coefficient Measurement of an ion in Pore Water of Granite and Tuff," J. Japan Soc. Engineering Geology, Vol.30, pp.84-90.
6. Kunori, S., Abe, M. and Saito, T., 1971, "Study on Weathering of Granitic Rocks (I)," Butsuri-Tanko, Vol.24, pp.6-17.
7. Lasaga, A.C., 1984, "Chemical Kinetics of Water-Rock Interactions," J. Geophys. Res., Vol.89, B6, pp.4009-4025.
8. Lin, F-C and Clemency, C.V., 1981, "Dissolution Kinetics of Phologopite. I. Closed System," Clays and Clay Minerals, Vol.29, pp.101-106.
9. Nakashima, S., 1987, "Infrared Microspectroscopy of Minerals: A New Microphase Characterization Technique in Earth Sciences," NihonDenshi News, Vol.27, 1-2, pp.12-17.
10. Nakashima, S. and Nakamura, H., 1987, "Mechanisms and Quantitative Evaluations of Radionuclide Fixation in Rocks and Sediments," Natural Analogues in Radioactive Waste Disposal. B. Come and N.A. Chapman, eds., Graham and Trotman, London, pp.386-396.
11. Nakayama, S. Moriyama, H, Arimoto, H. and Higashi, K., 1986,

"Behaviors of Americium in Aqueous Solutions Containing Iron," J. Nucl. Sci. Technol., Vol.23, pp.731-739.

12. Petit, J-C., Della Mea, G., Dran, J-C., Schott, J. and Berner, R.A., 1987, "Mechanism of Diopside Dissolution from Hydrogen Depth Profiling," Nature. Vol.325, 6106, pp.705-707.
13. Schwertmann, U., 1985, "The Effect of Pedogenic Environments on Iron Oxide Minerals," Advances in Soil Science, Vol.1, pp.171-200.
14. Sherman, D.M., Burns, R.G. and Burns, V.M., 1982, "Spectral Characteristics of the Iron Oxides with Application to the Martian Bright Region Mineralogy," J. Geophy. Res., Vol.87, B12, pp.10169-10180.
15. Smets, B.M.J. and Lommen, T.P.A., 1983, "The Role of Molecular Water in The Leaching of Glass," Phys. Chem. Glasses, Vol.24, pp.35-36.
16. Suzuki, T., Nakashima, S., Nagano, T. and Kita, H., 1989, "Micropore Distributions in Granite as Material Migration Pathways", Mining Geology, Vol.39 (in press)
17. Van der Marel, H.W. and Beutelspacher, H., 1976, "Atlas of Infrared Spectroscopy of Clay Minerals and their Admixtures," Elsevier, Amsterdam, 396p.
18. Van der Woude, J.H.A., Verhees, P. and De Bruyn, P.L., 1983, "Formation of Colloidal Dispersions fron Supersaturated Iron (III) Nitrate Solutions. II. Kinetics of Growth at Elevated Temperatures," Colloids and Surfaces, Vol.8, pp.79-92.
19. Vangenechten, J.H.D., Chughtai, N.A., Bierkens, J. and Vanderborght, O.L.J., 1987, "Similarity of ^{241}Am and ^{59}Fe Speciation in Selected Freshwaters and of Their Adsorption on Crayfish Exoskeleton," J. Environ. Radioactivity, Vol.5, pp.275-286.

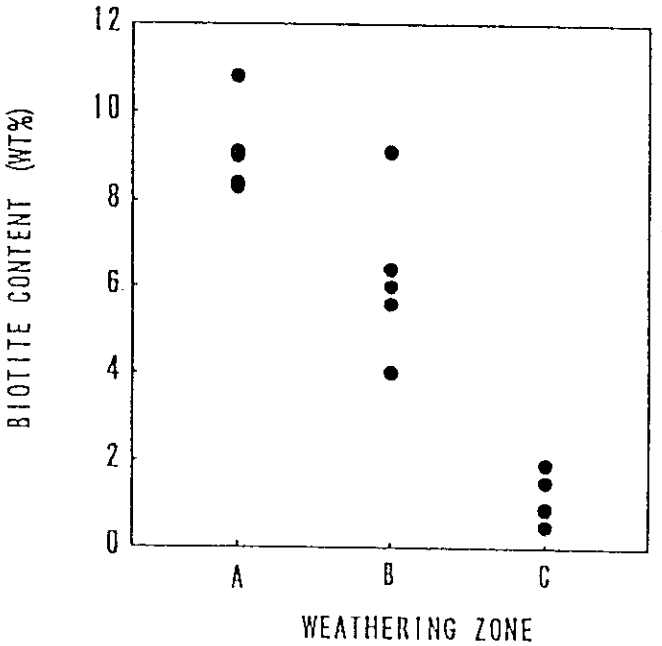

Fig. 1 Decrease of biotite content in weathered granitic rocks. The data were obtained by quantitative X-ray diffractometry on 18 powdered granitic rock samples from a cliff near Mizunuma Dam, Ibaraki, Japan. The rocks can be classified into three weathering zones with increasing weathering degrees from A to C (Kunori et al., 1971).

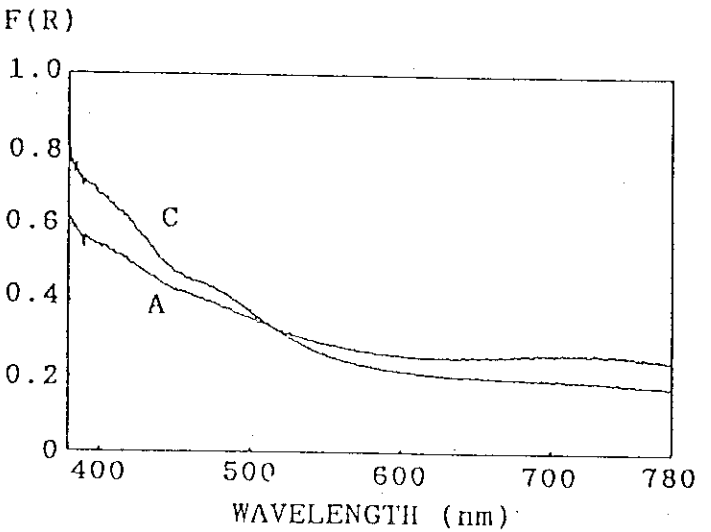

Fig. 2 Visible diffuse reflectance spectra of two typical weathered granitic rock samples. A weak broad band around 480 nm increases with the increase of weathering degree from the zone A to the zone C shown in Fig. 1. This band was attributed to the presence of FeO(OH) (cf. Fig. 3).

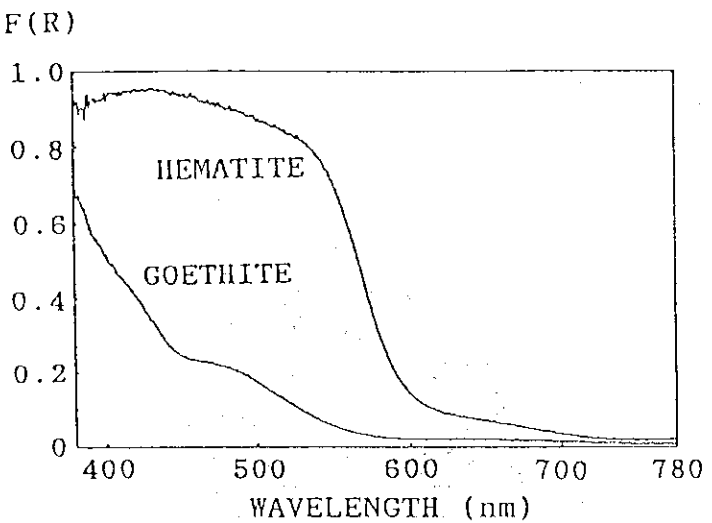

Fig. 3 Visible diffuse reflectance spectra of two typical ferric iron-bearing minerals. 0.78 wt% of hematite Fe_2O_3 and 1.67 wt% of goethite FeO(OH) are mixed with white Al_2O_3 respectively, for measuring these spectra.

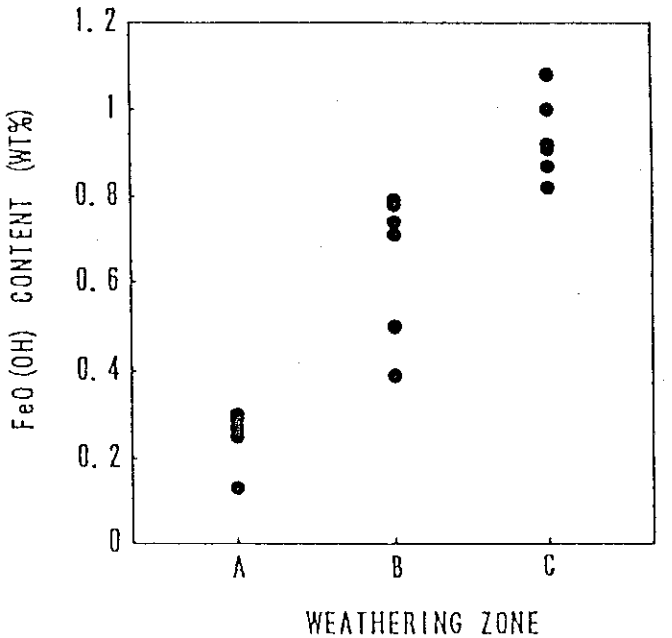

Fig. 4 Increase of FeO(OH) content in weathered granitic rocks shown in Fig. 1. The peak area around 480 nm of the visible diffuse reflectance spectra (Fig. 2) was assumed to represent FeO(OH) content of the powdered rock samples.

Fig. 5 Schematic drawing of the red coloration along a fracture of a granitic rock sample from Northwest Kyushu, Japan.
F : fracture filled mainly with prehnite
: feldspars with dots representing schematically the density of reddish color
: quartz
: greenish black minerals such as hornblende and chlorite

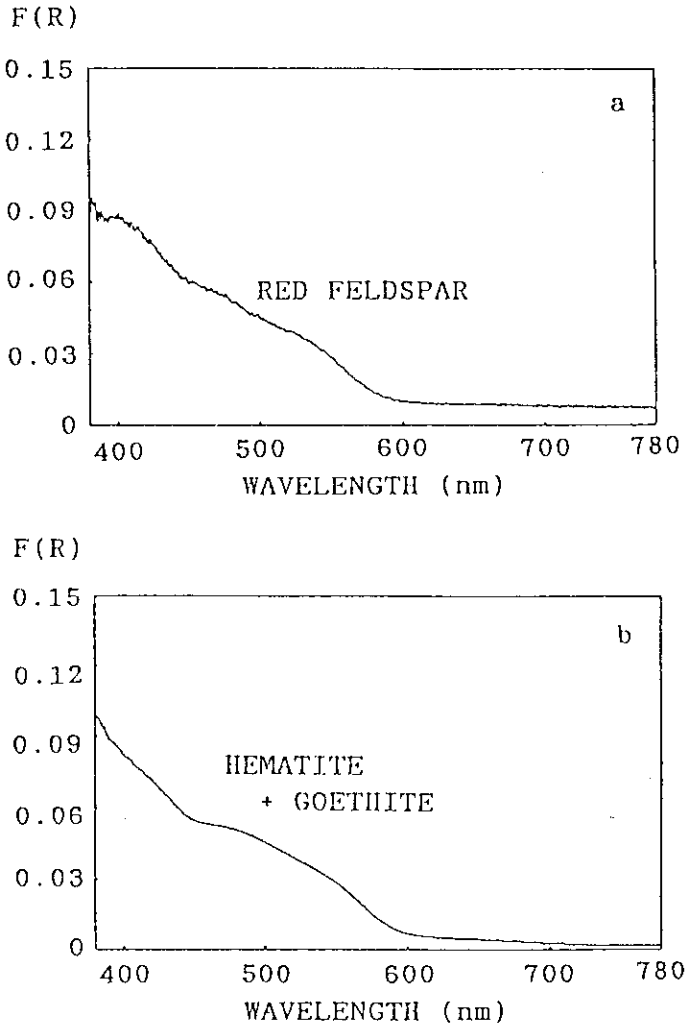

Fig. 6 (a) Visible diffuse reflectance spectrum of the red feldspar in the altered granitic rock shown in Fig. 5. (b) Visible diffuse reflectance composite spectrum of goethite plus hematite. This spectrum is fitted to that of the red feldspar (Fig.6a), and composed of 0.17 wt% of goethite and 0.03 wt%, of hematite in Al_2O_3.

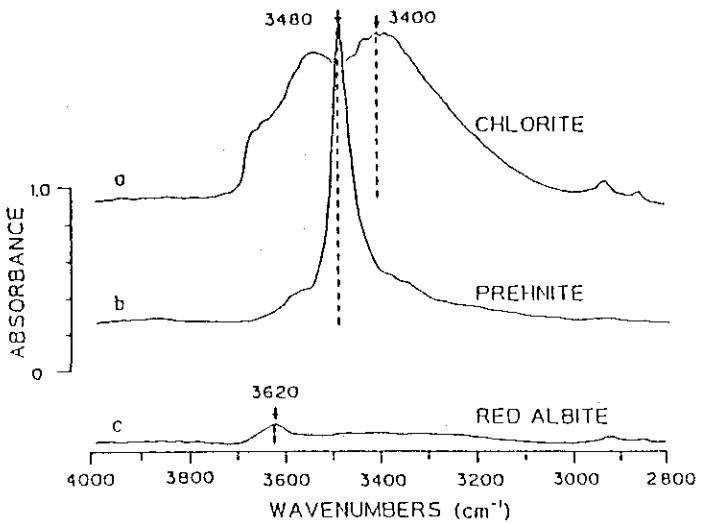

Fig. 7 Typical infrared transmission spectra for water in 10×10 μm area of three different minerals present in the red altered granitic rock shown in Fig. 5. Different states of O-H bond stretching are observed for these minerals. A weak peak at 3620 cm^{-1} for red albite is considered to be mainly due to sericite-like clays and a weak broad band around 3400 cm^{-1} in the same red albite can be due to OH of fine clays and/or OH incorpolated into the feldspar structure.

a: chlorite; $(Mg,Al,Fe)_{12}(Si,Al)_8O_{20}(OH)_{16}$

b: prehnite; $Ca_2(Al,Fe^{3+})_2Si_3O_{10}(OH)$

c: red feldspar; almost $NaAlSi_3O_8$ (albite)

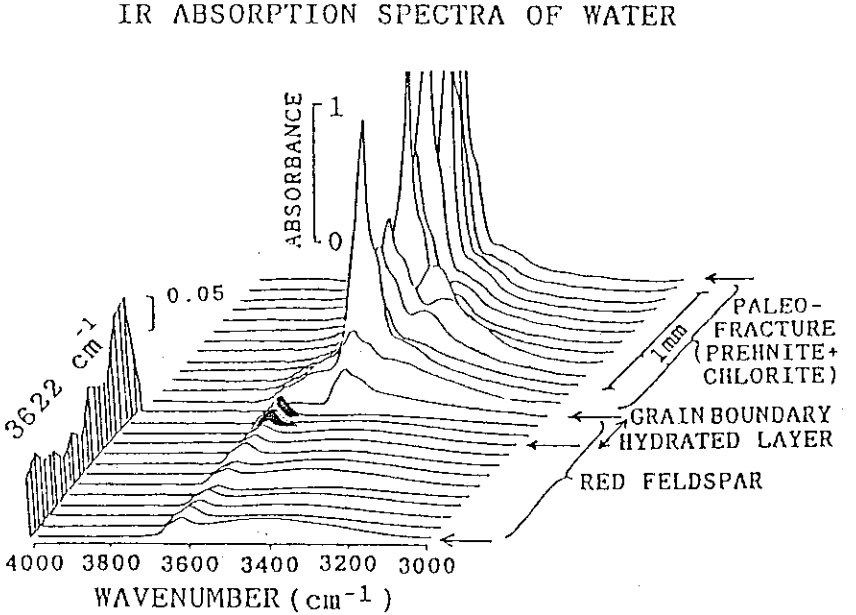

Fig. 8 Spectral results of a line-profile analysis by infrared microspectroscopy on the altered granitic rock shown in Fig. 5. Peak heights at 3622 cm^{-1} (possibly due to sericite-like clays) are projected with exaggeration on the left side. The surface 200 μm layer of a red feldspar grain appears to be enriched in water than the inner part. This layer is interpreted to be a hydrated surface layer of the red feldspar ajacent to the paleo-fracture.

2.3 Safety assessment methods for geological disposal

H. Nakamura

(1) Scenario and data base

In order to pick up the important items for the safety researches scenarios and data bases were listed.

a) Based scenario

The most probable release scenario and well known mechanisms were selected to assess the system performance at normal conditions.

b) Other scenarios

Unknown phenomena likely relevant to release were collected for sensitivity analysis of the phenomena and less probable phenomena were collected for assessment on abnormal conditions.

c) Data bases

- For preconditions: The combination of barriers, phenomena to be assessed, data regarding the waste form, capacity of repository and dominant functions of barriers for each period were reviewed.
- For based scenario: Recomended values of parameters in the based scenario were selected mainly from typical assessment reports such as Project Gewahr'85 and KBS-3. Results of relating experiments in our laboratory were also described briefly.
- For other scenarios: Probable values and/or the range of parameter were reviewed.

Table 1 summarizes the scenarios and the data bases.

(2) Rough estimation of ^{237}Np concentrations

Using the above scenarios and data bases and simple assumptions ^{237}Np concentrations and retardation periods in each barriers were estimated.

The results for the normal scenario are shown in Table 2. The dominant barrier for the retardation is the low permeable zone. The concentration will be decided mainly by dilution factor at high permeable zone. Table 3 shows results for low possible scenarios. The scenario of exposure of repository to ground surface after geotectonic movement is one of important scenario for long-term assessment where concentration factors of low soluble elements between the earth's crust and surface water or air were used for the calculation of transfer of ^{237}Np from soil to water or air. The

concentrations of ^{237}Np in the air are relatively higher than in water when they are compared with the values regulated for exhaust and drain respectively.

Table 1 Safety assessment scenario and data base

	Failure of Vessel	Migration in Engineered Barrier	Migration in Natural Barrier
1. Over all system	1) Based scenario corrosion of overpack - initiation just after closure - general corrosion	leaching from glass - soluble nuclides: leaching at the rate with the Si-saturated water - low soluble nuclides: convection of water and/or diffusion through pore water into rock matrix	retardation of migration in low permeable zone and dilution in permeable zone - low permeable zone: diffusion in pore and convection in fissure with diffusion to rock matrix - permeable zone: convection, diffusion and dilution both processes involve reversible adsorption
	2) Other scinario ($<10^3$ y) ①local failure of vessel ②human intrusion (not likely at <300y)	①leaching with high flow groundwater	(<10,000y) (>10,000y) ①fracture creation repository baring ②the sealing failure meteorite impact ③precipitation at discharging point
2. Subsystem	1) Based scinario corrosion in anoxic environment	normal condition - leaching with Si-saturated groundwater - saturation with low soluble nuclides - discharge to geosphere with convection and/or diffusion abnormal condition - leaching with high flow groundwater - discharge to geosphere with convection	- convection and diffusion for porous matrix - diffusion into rock matrix and dilution for fissure - reversible adsorption
	2) Other scinario ①local corrosion: stress corrosion cracking pit corrosion ②acceleration of general corrosion: irradiation, biology ③change of environment: seepaging of oxidic water	①change of leach rate and/or solubility with the change of altered layer on glass ②conversion of leached nuclides to non-precipitable species ③change of leach rate with following factors fracturing, recrystalization, radiation damage of glass matrix, radiolisis of water	①mineralization ②slow reaction of adsorption and desorption ③conversion to non-sorbiong species ④time dependency of following parameters: dilution factor, hydrolic head gradient, diffusion coefficient, chemical composition
3. Data base	1) For precondition ①concept of repository ②potential phenomena relevant to release ③waste generation ④termination of assessment period	⑤composition of the waste ⑥canister ⑦overpack	(㉒critical values of parameters relevant to select a dominant scenario: flow rate, thickness of low permeable zone, dilution and travel time, distance from high slopes and depth from the ground surface)
	2) For based scinario ⑧seepage of groundwater: just after closure ⑨corrosion rate: iron 5cm/1000y, titanium 0.5mm/1000y	⑪high leach rate: 5×10^{-4} g/cm^{2}d 90°C ⑫leach rate with Si-water: 1×10^{-7} g/cm^{2}d 70°C Q = 65 kJ/mol ⑬sat. conc.: Pu 1×10^{-8} Np 4×10^{-9} mol/l Am 2×10^{-7} Tc 3×10^{-7} mol/l	⑰groundwater properties: the tipical properties of sea water and surface water enclosed in old age ⑱hydraulic conductivity: granite 1×10^{-12} fracture 1×10^{-9} m/s ⑲diffusion coefficient: granite 1×10^{-12} fracture 1.5×10^{-10} m^2/s buffer 1×10^{-10} soil 5×10^{-10} m^2/s ⑳distribution coefficient: low Kd = measured values, high Kd>10^3 = 10^3 layer thickness, gradient: site specific data
	3) Other scinario ⑩local failure: no barrier function just after introduction of failing condition	⑭effects of altered layer of glass: change of solubility with the alteration ⑮conversion to moval species: <0.1% ? ⑯acceleration of leaching with various factors: less than 10 times	㉑mineralization rate: $T_{1/2}$ = 2 ~ 10^6 y ㉒conversion to nonsorbing species: ~1% ? ㉓change of geologic data by rare phenomena: conductivity; nonfracture rock to fracture, discharge point; to sea and/or land

Table 2 Times for passing through barriers and concentration at outside border of barriers (^{237}Np)

	package (cast iron)	waste form (borosilicate glass)	buffer material (bentonite)	low permeable zone (fine fissure)	permeable zone (fracture)
precondition	thickness(X_V) 25 cm	diameter(r_G) 42 cm spesific gravity(ρ_G) 2.8 g/cm^3 concentration of ^{237}Np(C_G) 1 μCi/g	thickness(X_B) 30 cm head gradient(G_B) 0.0	thickness(X_L) 100m head gradient(G_L) 0.01	thickness(X_H) 500m head gradient(G_H) 0.05
scenario	general corrosion	leaching and precipitation	one dimentional diffusion & adsorption	one dimentional convection & adsorption	one dimentional convection adsorption & dilution
	general corrosion rate(L_V) 0.05mm/y	solubility of ^{237}Np(S_{NP})4×10^{-9}mol/l (6.6×10^{-7} μCi/ml) leach rate(L_{GS}) 1×10^{-7}g/cm^{2}d half life of ^{237}Np 2.1×10^{6}y	diffusion coefficient (D_B) 1×10^{-10}m^2/s retardation fact.(R_B) 200 porosity(ε_B) 0.5	hydraulic conductivity (K_L) 1×10^{-9}m/s retardation fact.(R_L) 200 porosity(ε_L) 0.01	hydraulic conductivity (K_H) 1×10^{-5}m/s retardation fact.(R_H) 200 porosity(ε_H) 0.1
time for pass(t) calculation forms	$t = X_V/L_V$	$t_G = 0$	$t_B = X_B^2 R_B/4D$	$t_L = \varepsilon_L X_L R_L/K_L G_L$	$t_H = \varepsilon_H X_H R_H/K_H G_H$
calculated time for pass	5,000 y	0 y	1.4×10^3 y[1)]	6.3×10^5 y	6.3×10^2 y
dilution ratio	1	1	1	1	$\varepsilon_H X_H t_L/\varepsilon_L X_L t_H$ = 500
concentration[2)]	0	6.6×10^{-7} μCi/ml	6.6×10^{-7} μCi/ml	5.3×10^{-7} μCi/ml	1.1×10^{-11} μCi/ml

1) Concentration of radionuclides is expressed by $C = C_o \mathrm{erfc}(X_B/2\sqrt{D_B t/R_B})$.
The time for $1 = X_B/2\sqrt{D_B t/R_B}$ is defined as the time for pass.
2) Calculated using dilution rate and disintegration rate.

Table 3 Scenarios of low probability

a) Drinking scenario

Scenarios	Data base	assumption for calculation	formula	result
drilling for well passing through glass	diameter of a drill(r_B) 10cm length of drilled glass(X_G) 1m volume of drinking water(Q_W) 1m^3/d high leach rate(L_{GH}) 3×10^{-5}g/d	Class is leached from wall of drilling. Sorption during pomping up is neglected.	$\frac{\pi(r_B/2)^2 X_G L_{GH} C_G}{Q_W}$	2×10^{-9} μCi/ml
failure of sealing and release of groundwater	volume of released water(Q_S) 1m^3/d surface area of glass(SA_G) 1m^2/canister	Glass is leached from all of surface and Sorption during seepaging is neglected.	$\frac{SA_G L_{GH} C_G}{Q_S}$	3×10^{-7} μCi/ml
exposure of repository weathered to soil	thickness of repository(X_R) 10m concentration factor of water/soil(K_{DS}) 10^{-5} disposal density(N_G) $10^{-2}/m^2$	The repository is exposed in biosphere. weathered to soil and dipersed to air.	$\frac{\pi(r_B/2)^2 X_G C_G \rho_G K_{DS} N_G}{X_R}$	4×10^{-9} μCi/ml

b) Inhalation

Scenarios	Data base	assumption for calculation	formula	result
Dispersion of glass powder produced by drilling	dispersion area(SD_G) 10^2m^2 dispersion index(I) $2\times10^{-8}cm^{-1}$	Glass powder formed by drilling disperses in the pond, drys and disperses.	$\frac{X_D \pi r_B X_G C_G \rho_G I}{SD_G}$	2×10^{-10} μCi/cm^3
exposure of repository weathered to soil	concentration factor between air and the earth crust(I_G) 3×10^{-11}	The repository is weathered and becomes homogeneous soil which dispersed as soil.	$\frac{\pi(r_B/2)^2 X_G C_G \rho_G I_G N_G}{X_R}$	1×10^{-14} μCi/cm^3
meteor impact	distance of dispersion(X_A) 10km dispersion ratio(Ip) 1×10^{-4}	All of the repository diperses by the same rate as glass powder dispersion when the waste dropes in a storage.	$\frac{\pi(r_B/2)^2 X_G C_G \rho_G I_P N_G}{X_A}$	4×10^{-11} μCi/cm^3

3. Hot operation at WASTEF

M. Senoo

In the WASTEF (Waste Safety Testing Facility), hot examinations have been continued on the performance and long-term durability of HLW solidified forms and the related materials in storage and disposal conditions.

Using the actual high level liquid waste, which was transported from Power Reactor and Nuclear Fuel Development Corporation (PNC) in the last year, the safety examinations of waste forms have been initiated.

In Table 1, vitrified forms using actual waste were shown by serial number with "A88...".

Accelerated alpha radiation stability tests on Synroc forms were being continued, and the samples of up to 1000 years equivalent aging to actual waste were examined.

Besides the two topics above mentioned, leaching tests of various radionuclide, accelerated alpha radiation stability tests, and various activities supporting the safety examinations have been continued.

Table 1 Vitrified form production

Serial Number	Volume	Radionuclides in the Forms	The Purpose of Vitrification
A88001	0.33l	Cs-134,Cs-137 etc. (total 526 Ci)	Solidification test of actual waste
A88002	0.8 l	Cs-134,Cs-137 etc. (total 2,920 Ci)	Solgification test of actual waste
A88003	8.3ml	Cm-244 (6.3 Ci) HLW (30 Ci)	Alpha-radiation stability test (IV)
A88004	8.3ml	Cm-244 (6.3 Ci) HLW (30 Ci)	Alpha-radiation stability test (IV)
A88005	8.3ml	Cm-244 (6.3 Ci) HLW (30 Ci)	Alpha-radiation stability test (IV)
A88006	8.3ml	Cm-244 (6.3 Ci) HLW (30 Ci)	Alpha-radiation stability test (IV)
A88007	3.5ml	Cm-244 (2.7 Ci) HLW (11 Ci)	Alpha-radiation stability test (IV)
H88001	22 ml	Pu-238 (0.54 g)	Leachability examination
H88002	22 ml	Pu-238 (0.54 g)	Leachability examination
H88003	9 ml	Pu-238 (0.23 g)	Leachability examination

(i) Transport Packaging for the HLW Glass Sample

JAERI is planning to the tranportation of the HLW glass sample from USNRC to WASTEF for the joint research by JAERI and USNRC. For that purpose, WASTEF planned to fabricate the packaging for HLW glass sample and design work of the packaging (VFC-88Y-2T type packaging see Fig. 1) has been completed.

In designing of the packaging, consideration is given to making the design of the structure as simple as possible in order to facilitate handling and decontamination in the hot cell. In addition, the packaging is to be so designed as to have small inner space and thick shielding because the HLW glass sample is very small but its radioactive concentration is rather high.

Specially, the body of packaging is made of a stainless steel ingot into which a hole is bored through its central section. As a result, structure integrating a body with a bottom and therefore has no welding joint is obtained. This structure also aims to realize the quality assurance regarding fabrication and to facilitate manufacturing. In addition, a double containment was employed, which consists of inner capsule containing the glass sample and the cask body (exterior container) containing the former. The cask body does not have many projections except for the parts required for tie-down, and is provided with bolts and tie-down device to avoid a direct primary impact under the drop test condition. The cask body, bottom, and cask lid function as shields with a sufficient thickness. The packaging has no shock absorber and a protecting cover is provided on the cask lid.

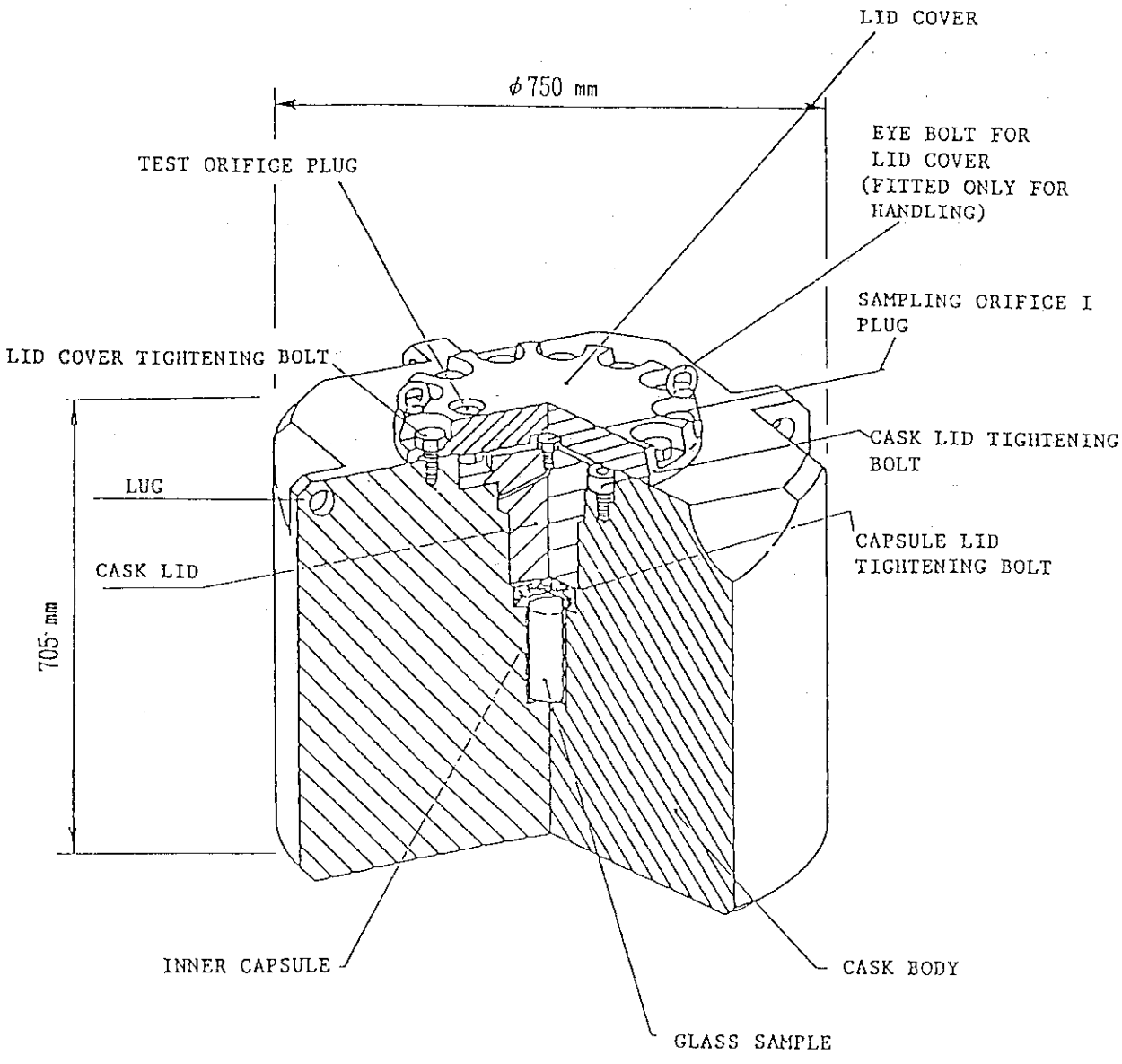

Fig. 1 Bird's-Eye View of VFC-88Y-2T

(ii) Safety Demonstration Test on Enclosing Performance of Vitrified Form

Based on a requirement from STA (Science and Technology Agency), a test for evaluating performance of enclosing of HLW vitrified form was started to demonstrate the safety of HLW storage facility. In Japan, two storage facilities are being planned for HLW vitrified forms, one is under construction by PNC (Power and Nuclear Fuel Development Corporation) at Tokai-mura, and the other is being planned by JNFS (Japan Nuclear Fuel Service Co., Ltd) at Rokkasho-mura in Aomori Prefecture.

In the test, volatility of ^{137}Cs and ^{106}Ru is to be measured under the normal and accidental conditions of the storage facilities. The samples to be used in the demonstration test will be prepared in 1989 using actual high level liquid waste to be transported from Tokai Reprocessing Plant of PNC.

In the last fiscal year (1988), survey was performed on the basic data for evaluating volatility, examples of safety analysis for enclosing against volatile materials in storage facility, and method for enclosing at several foreign storage facilities.